arXiv:cond-mat/0608690v2 [cond-mat.str-el] 19 Nov 2006

Modern Physics Letters B
© World Scientific Publishing Company

Hidden symmetry and quantum phases in spin-3/2 cold atomic systems

Congjun Wu
Kavli Institute for Theoretical Physics, University of California,
Santa Barbara, CA 93106, USA.
wucj@kitp.ucsb.edu

Received (Day Month Year)
Revised (Day Month Year)

Optical traps and lattices provide a new opportunity to study strongly correlated high spin systems with cold atoms. In this article, we review the recent progress on the hidden symmetry properties in the simplest high spin fermionic systems with hyperfine spin $F = 3/2$, which may be realized with atoms of ^{132}Cs, ^{9}Be, ^{135}Ba, ^{137}Ba, and ^{201}Hg. A *generic* $SO(5)$ or isomorphically, $Sp(4)$) symmetry is proved in such systems with the *s*-wave scattering interactions in optical traps, or with the on-site Hubbard interactions in optical lattices. Various important features from this high symmetry are studied in the Fermi liquid theory, the mean field phase diagram, and the sign problem in quantum Monte-Carlo simulations. In the *s*-wave quintet Cooper pairing phase, the half-quantum vortex exhibits the global analogue of the Alice string and non-Abelian Cheshire charge properties in gauge theories. The existence of the quartetting phase, a four-fermion counterpart of the Cooper pairing phase, and its competition with other orders are studied in one dimensional spin-3/2 systems. We also show that counter-intuitively quantum fluctuations in spin-3/2 magnetic systems are even stronger than those in spin-1/2 systems.

Keywords: high spin; hidden symmetry; quintet Cooper pairing; quartetting.

1. Introduction

The past decade has witnessed the great progress in the cold atomic physics. The first generation of Bose-Einstein condensation (BEC) in alkali atoms was realized in magnetic traps. In such systems, spins of atoms are fully polarized by the Zeemann field [1,2], thus atoms are effectively of single component. A few years later, important achievement was made to release the spin degrees of freedom by using optical methods to trap atoms, such as optical traps and lattices [3,4,5]. An additional advantage of optical lattices is the excellent controllability of the interaction strength from the weak coupling to strong coupling regimes. For example, the superfluid to Mott insulator transition of bosons has been experimentally observed [6]. All these progresses provide a controllable way to study high spin physics, in particular, the strongly correlated high spin physics.

The high spin physics with cold atoms contains novel features which does not appear in solid state systems. In many transition metal oxides, several electrons are combined by Hund's rule to form an onsite composite high spin object with $S > \frac{1}{2}$. However, the intersite coupling is still dominated by the exchange process of a single pair of electrons, thus the leading order spin exchange is the bilinear Heisenberg term. Due to the $1/S$ effect, quantum fluctuations are typically weak. In other words, the solid state high spin systems are more classical than spin-$\frac{1}{2}$ systems. In contrast, such restriction does not happen in high spin systems with cold atoms because the building block of such systems, each atom, carries a high hyperfine spin F which includes both electron and nuclear spins. This feature renders the possible high hidden symmetries and strong quantum fluctuations.

The high spin bosonic systems exhibit much richer phase diagram than the spinless boson. In spin-1 systems of ^{23}Na and ^{87}Rb atoms, polar and ferromagnetic spinor condensations and related collective modes were studied by Ho [7] and Ohmi *et al* [8]. The interplay between the $U(1)$ charge and $SU(2)$ spin degrees of freedom in the spinor condensate is characterized by a Z_2 gauge symmetry. The topological aspect of this hidden Z_2 gauge symmetry was investigated extensively by Zhou [9,10] and Demler *et al* [11]. Furthermore, the spin singlet state and spin nematic state were also studied in optical lattices by Zhou *et al.* [12] and Imambekov *et al* [13]. Recently, the spin-2 hyperfine state of ^{87}Rb atom [14,15] and spin-3 atom of ^{52}Cr [16,17,18,19] have attracted a lot of attention. Various spinor condensates and spin ordered Mott insulating states have been classified. Remarkably, a biaxial spin-nematic state can be stabilized in ^{52}Cr systems which can support interesting topological defects of non-Abelian vortices.

On the other hand, relatively less works have been done for high spin fermions. However, such systems indeed have interesting properties, and thus deserve attention. Pioneering works by Yip *et al.* [20] and Ho *et al.* [20] showed that high spin fermionic systems exhibit richer structures of collective modes in the Fermi liquid theory, and more diversities in Cooper pairing patterns. More recently, a large progress has been made by Wu *et al.* [21] on the symmetry properties in spin-3/2 systems, which may be realized with atoms such as ^{132}Cs, ^{9}Be, ^{135}Ba, ^{137}Ba, ^{201}Hg. Such systems are very special in that in additional to the obvious spin $SU(2)$ symmetry, they possess a hidden and *generic* $SO(5)$ or isomorphically, $Sp(4)$ symmetry. In this paper, we will review this progress.

Before we move on, let us briefly review some group theory knowledge. The $SO(5)$ group describes the rotation in the 5-dimensional space spanned by five real axes $n_1 \sim n_5$ which form the vector representation of $SO(5)$. $SO(5)$ group has ten generators L_{ab} $(1 \leq a < b \leq 5)$, each of which is responsible for the rotation in the ab plane. These generators form $SO(5)$'s 10 dimensional adjoint representation. $SO(5)$'s fundamental spinor representation is 4-dimensional. Rigorously speaking, its spinor representation is faithful for $SO(5)$'s covering group $Sp(4)$. The relation between $SO(5)$ and $Sp(4)$ is similar to that between $SO(3)$ and $SU(2)$. For simplicity, we will not distinguish the difference between $SO(5)$ and $Sp(4)$ below.

The origin of the $SO(5)$ symmetry in spin-3/2 systems can be explained as follows: The kinetic energy term shows an obvious $SU(4)$ symmetry because of the equivalence among the four spin components $\psi_\alpha(\alpha = \pm\frac{3}{2}, \pm\frac{1}{2})$. However, this $SU(4)$ symmetry generally speaking is broken explicitly down to $SO(5)$ by interactions. Pauli's exclusion principle requires that in the s-wave scattering channel, only interactions g_0 in the total spin singlet channel ($S_T = 0$) and g_2 in the quintet channel ($S_T = 2$) are allowed, while those in the channels of $S_T = 1, 3$ are forbidden. Remarkably, the singlet and quintet channels automatically form the identity and 5-vector representations for an $SO(5)$ group (see Sect. 2 for detail), thus making the system $SO(5)$ invariant without fine tuning. The same reasoning also applies to the existence of the $SO(5)$ symmetry in the lattice Hubbard model. The validity of this $SO(5)$ symmetry is regardless of dimensionality, lattice geometry and impurity potentials. Basically, it plays the same role of the $SU(2)$ symmetry in the spin-$\frac{1}{2}$ systems. This $SO(5)$ symmetry purely lies in the particle-hole channel as an extension of the spin $SU(2)$ algebra. It is qualitatively different from the $SO(5)$ theory in the high T_c superconductivity [22] which involves both particle-hole and particle-particle channels.

To our knowledge, such a high symmetry without fine tuning is rare in condensed matter and cold atomic systems, and thus it is worthwhile for further exploration. Below we outline several important consequences from the $SO(5)$ symmetry and other interesting properties in spin-3/2 systems. The $SO(5)$ symmetry brings hidden degeneracy in the collective modes in the Fermi liquid theory [21]. This symmetry greatly facilitates the understanding of the mean field phase diagram in the lattice system [21]. Furthermore, due to the time-reversal properties of the $SO(5)$ algebra, the sign problem of the quantum Monte-Carlo algorithm is proved to be absent in a large part of the phase diagram [21,23].

Spin-3/2 systems can support the quintet Cooper pairing phase i.e., Cooper pair with total spin $S_{tot} = 2$. This high spin superfluid state possesses the topological defect of the half-quantum vortex often called the Alice string. An interesting property of the half quantum vortex loop or pair is that they can carry spin quantum number as a global analogy of the Cheshire charge in the gauge theories. Interestingly, in the quintet pairing state, when a quasiparticle carrying spin penetrates the Cheshire charged half-quantum vortex loop, quantum entanglement is generated between them. The Alice string and non-Abelian Cheshire charge behavior in spin-3/2 systems were studied by Wu *et al* [24].

Fermionic systems with multiple components can support multiple-particle clustering instabilities, which means more than two fermions come together to form bound states [25,26,27,28,29,30,31]. For example, baryons are bound states of three-quarks, α-particles are bound states of two protons and two neutrons, and bi-excitons are bound state of two electrons and two holes. Spin-3/2 systems can exhibit quartetting order as a four-fermion counterpart of the Cooper pairing. Taking into account the arrival of the fermion pairing superfluidity by Feshbach resonances [32,33,34,35], it is natural to expect the quartetting order as a possible research focus in the near future. The existence of the quartetting order and its competition with the singlet pairing order were investigated by Wu [28] in 1D spin-3/2 systems. The generalization of the quartetting order to even higher spin systems at 1D was investigated by Lecheminant *et al* [36].

Spin-3/2 magnetic systems are characterized by strong quantum fluctuations. This is a little bit counter-intuitive because one would expect weak quantum fluctuations due to the high spin. However, because of the high symmetry of $SO(5)$, quantum fluctuations are actually even stronger than those in spin $\frac{1}{2}$ systems. For example, spin-3/2 systems at quarter filling (one particle per site) can exhibit the $SU(4)$ plaquette order which is a four-site counterpart of the dimer state in spin-$\frac{1}{2}$ systems. An $SU(4)$ Majumdar-Ghosh model was constructed by Chen *et al.* [37] in the spin-3/2 two-leg ladder systems. Their ground state is exactly solvable and exhibits such plaquette order.

On the experimental side, in addition to alkali atoms, considerable progress has been made in trapping and cooling the divalent alkaline-earth atoms [38,39,40,41]. Two candidate spin-3/2 atoms are alkaline-earth atoms of ^{135}Ba and ^{137}Ba. Their resonances of $6s^2 \rightarrow 6s^1 6p^1$ are at 553.7 nm [42], thus making them as promising candidates for laser cooling and further experimental investigation. Their scattering lengths are not available now, but that of ^{138}Ba (spin 0) was estimated as $-41a_B$ [38]. Because the $6s$ shell of Ba is fully-filled, both the a_0, a_2 of ^{135}Ba and ^{137}Ba should have the similar value. Considering the rapid development in this field, we expect that more spin-3/2 systems can be realized experimentally.

In the rest of this paper, we will review the progress in spin-3/2 system, and also present some new results unpublished before. In Sect. 2, we introduce the proof of the exact $SO(5)$ symmetry. In Sect. 3, we present the effect of the $SO(5)$ symmetry to the spin-3/2 Fermi liquid theory, the mean field phase diagram of the lattice Hubbard model, and the sign problem of quantum Monte Carlo sign problem. In Sect. 4, we review the quintet Cooper pairing and the topological defect of the half-quantum vortex. In Sect. 5 we discuss the quartetting instability and its competition with pairing instability in 1D systems. In Sect. 6, we study the spin-3/2 magnetism. We summarize the paper in Sect. 7.

Due to limitation of space, we will not cover several important works on the spin-3/2 fermions. For example, Hattori [43] studied the Kondo problem finding an interesting non-Fermi liquid fixed point. Recently, the 1D spin-3/2 model with arbitrary interactions was solved using Bethe-ansatz by Controzzi *et. al* [44].

2. The hidden $SO(5)(Sp(4))$ symmetry

In this section, we will review the hidden symmetry properties of spin-3/2 systems [21,23]. Let us first look at a familiar example of hidden symmetry: the hydrogen atom. The hydrogen atom has an obvious $SO(3)$ symmetry which can not explain the large energy level degeneracy pattern of n^2. Actually, this degeneracy is not accidental. It arises from the $1/r$ Coulomb potential which gives rise to a hidden conserved quantity, the Runge-Lentz (R-L) vector. This vector describes the orientation and eccentricity of the classical elliptic orbits. The R-L vector and orbital angular momentum together form a closed $SO(4)$ algebra which is responsible for the degeneracy pattern of n^2. Now we can ask: what are the hidden conserved quantities in spin-3/2 systems? We will answer this question below.

2.1. *Model Hamiltonians*

We start with the generic form of the spin-3/2 Hamiltonian of the continuum model [45,20]. The only assumptions we will make are the spin $SU(2)$ symmetry and the s-wave scattering interactions. Required by Paul's exclusion principle, the spin channel wave function of two fermions has to be antisymmetric in the s-partial wave channel. As a result, only two independent interaction channels exist with the total spin $F = 0, 2$. Taking the above facts into account, the Hamiltonian reads

$$H = \int d^d\vec{r}\, \Big\{ \sum_{\alpha=\pm 3/2, \pm 1/2} \psi^\dagger_\alpha(\vec{r})\big(-\frac{\hbar^2}{2m}\nabla^2 - \mu\big)\psi_\alpha(\vec{r}) + g_0 P^\dagger_{0,0}(\vec{r}) P_{0,0}(\vec{r}) \\ + g_2 \sum_{m=\pm 2,\pm 1, 0} P^\dagger_{2,m}(\vec{r}) P_{2,m}(\vec{r}) \Big\}, \tag{1}$$

with d the space dimension, μ the chemical potential. $P^\dagger_{0,0}, P^\dagger_{2,m}$ are the singlet ($S_T = 0$) and quintet ($S_T = 2$) pairing operators defined through the Clebsh-Gordan coefficient for two indistinguishable particles as $P^\dagger_{F,m}(\vec{r}) = \sum_{\alpha\beta} \langle \frac{3}{2}\frac{3}{2}; F, m | \frac{3}{2}\frac{3}{2}\alpha\beta \rangle \psi^\dagger_\alpha(\vec{r}) \psi^\dagger_\beta(\vec{r})$, where $F = 0, 2$ and $m = -F, -F+1, ..., F$. The feature that only two interaction channels exist is important for the existence of the hidden $SO(5)$ symmetry.

If spin-3/2 atoms are loaded into optical lattices, we need to construct the lattice Hamiltonian. We assume V_0 the potential depth , $k = \pi/l_0$ the light wavevector, and l_0 the lattice constant. The hopping integral t decreases exponentially with increasing V_0. Within the harmonic approximation, $U/\Delta E \approx (\pi^2/2)(a_s/l_0)(V_0/E_r)^{1/4}$, with U the repulsion of two fermions on one site, ΔE the gap between the lowest and first excited single particle state in one site, a_s the s-wave scattering length in the corresponding channel, and $E_r = \hbar^2 k^2/2M$ the recoil energy. In the absence of Feshbach resonances, the typical estimation reads $a_s \sim 100 a_B$ (a_B the Bohr radius), $l_0 \sim 5000$A, and $(V_0/E_r)^{1/4} \approx 1 \sim 2$. Thus we arrive at $U/\Delta E < 0.1$, and the system can be approximated by the one-band Hubbard model

$$H = -t \sum_{\langle ij \rangle, \sigma} \{ c^\dagger_{i\sigma} c_{j\sigma} + h.c. \} - \mu \sum_{i\sigma} c^\dagger_{i\sigma} c_{i\sigma} + U_0 \sum_i P^\dagger_{0,0}(i) P_{0,0}(i) \\ + U_2 \sum_{i, m=\pm 2, \pm 1, 0} P^\dagger_{2,m}(i) P_{2,m}(i). \tag{2}$$

for the particle density $n \leq 4$. At half-filling in a bipartite lattice, μ is given by $\mu_0 = (U_0 + 5U_2)/4$ to ensure the particle-hole (p-h) symmetry. The lattice fermion operators and their continuum counterparts are related by $\psi_\alpha(\vec{r}) = c_\alpha(i)/(l_0)^{d/2}$.

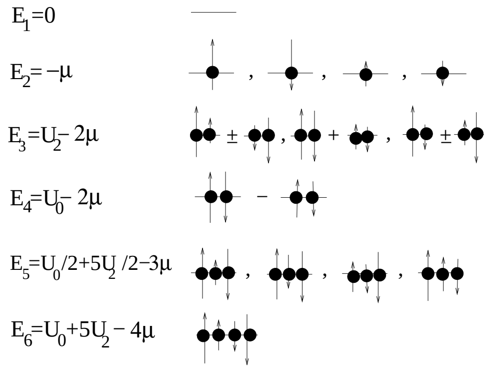

Fig. 1. Energy level diagram for a single site problem. The longer and shorter arrows denote the spin components of $S_z = \pm\frac{3}{2}$ and $S_z = \pm\frac{1}{2}$ respectively. The sets of $\mathrm{E}_{1,4,6}$ (spin singlet) are also $SO(5)$ singlet; $\mathrm{E}_{2,5}$(spin quartet) are $SO(5)$ spinors; E_3 (spin quintet) is an $SO(5)$ vector.

The best way to understand the $SO(5)$ symmetry without going through the mathematical details is to look at the energy level diagram for the single site problem as depicted in Fig. 1. It contains 2^4=16 states which can be classified into three sets of spin singlets ($E_{1,4,6}$), two sets of spin quartets ($E_{2,5}$), and one set of spin quintet (E_3). Interestingly, this energy level degeneracy pattern matches $SO(5)$ representations perfectly: the spin singlets $E_{1,4,6}$, quartets $E_{2,5}$, and quintet E_3 can be considered as $SO(5)$ singlets, spinors, and vector as well. Thus the single site spectrum is $SO(5)$ symmetric without any fine tuning. If we further tune $U_0 = U_2 = U$, then $E_{3,4}$ become 6-fold degenerate making the system $SU(4)$ invariant. In this case, interactions in Eq. 2 reduce to the density-density interaction as $H_{int} = \frac{U}{2}n(n-1)$. The $SU(4)$ symmetry simply means that the four spin-components are equivalent to each other.

2.2. *The particle-hole channel SO(5) algebra*

In order to prove the $SO(5)$ symmetry in the many-body Hamiltonians of Eq. 1 and 2, we need to construct the $SO(5)$ algebra. The four spin components $\psi_\alpha(\vec{r})(\alpha = \pm\frac{3}{2}, \pm\frac{1}{2})$ render $4^2 = 16$ p-h channel bi-linears. As a result, the charge operator and three spin $F_{x,y,z}$ operators are not a complete set for describing the total degrees of freedom. High order tensors are needed in terms of the tensor product of $s = 3/2$ spin matrices F_i:

$$\begin{aligned}
&\text{rank-0: } I, \\
&\text{rank-1: } F^i, \quad i = 1, 2, 3, \\
&\text{rank-2: } \xi^a_{ij} F_i F_j, \quad a = 1, .., 5, \quad \xi^a_{ij} = \xi^a_{ji}, \quad \xi^a_{ii} = 0, \\
&\text{rank-3: } \xi^L_{ijk} F_i F_j F_k, \quad L = 1, .., 7, \quad \xi^L_{ijk} = \xi^L_{jik}, \quad \xi^L_{iik} = 0,
\end{aligned} \tag{3}$$

where ξ^a_{ij} and ξ^a_{ijk} are fully symmetric, traceless tensors with the detailed forms given in Ref. [46].

The five rank-2 tensors are often denoted as spin-nematic matrices. They are

$$\begin{aligned}\Gamma^1 &= \frac{1}{\sqrt{3}}(F_xF_y+F_yF_x), \quad \Gamma^2 = \frac{1}{\sqrt{3}}(F_zF_x+F_xF_z), \quad \Gamma^3 = \frac{1}{\sqrt{3}}(F_zF_y+F_yF_z), \\ \Gamma^4 &= \frac{1}{\sqrt{3}}(F_z^2-\frac{5}{4}), \qquad\qquad \Gamma^5 = \frac{1}{\sqrt{3}}(F_x^2-F_y^2). \end{aligned} \tag{4}$$

Remarkably, for $F=\frac{3}{2}$, they anticommute with each other and form a basis of the Dirac Γ matrices as $\{\Gamma_a,\Gamma_b\}=2\delta_{ab}$, i.e., they form an $SO(5)$ vector. More explicitly, they are expressed as

$$\Gamma^1 = \begin{pmatrix} 0 & -iI \\ iI & 0 \end{pmatrix}, \quad \Gamma^{2,3,4} = \begin{pmatrix} \vec\sigma & 0 \\ 0 & -\vec\sigma \end{pmatrix}, \quad \Gamma^5 = \begin{pmatrix} 0 & I \\ I & 0 \end{pmatrix}, \tag{5}$$

where I and $\vec\sigma$ are the 2× 2 unit and Pauli matrices. On the other hand, three spin operators $F_{x,y,z}$ and seven rank-3 spin tensors $\xi^L_{ijk}F_iF_jF_k, (L=1,..,7)$ together form the ten $SO(5)$ generators. By linear combinations, these generators can be organized into

$$\Gamma^{ab} = -\frac{i}{2}[\Gamma^a,\Gamma^b] \quad (1\le a,b\le 5). \tag{6}$$

Consequently, the 16 bilinear operators can also be classified according to their properties under the $SO(5)$ transformations as scalar n (density), vector n_a (spin nematics), and anti-symmetric tensors L_{ab} (spin and spin cubic tensors):

$$\begin{aligned} n(\vec r) &= \psi^\dagger_\alpha(\vec r)\psi_\alpha(\vec r), \quad n_a(\vec r) = \frac{1}{2}\psi^\dagger_\alpha(\vec r)\Gamma^a_{\alpha\beta}\psi_\beta(\vec r), \\ L_{ab}(\vec r) &= -\frac{1}{2}\psi^\dagger_\alpha(\vec r)\Gamma^{ab}_{\alpha\beta}\psi_\beta(\vec r). \end{aligned} \tag{7}$$

L_{ab} and n_a together form the $SU(4)$, or isomorphically, the $SO(6)$ generators. The n, n_a, and L_{ab} in the lattice model can also be defined accordingly.

Next we study the particle-particle channel bilinears. Pairing operators can be organized as $SO(5)$ scalar and vector operators through the charge conjugation matrix $R=\Gamma_1\Gamma_3$ as

$$\begin{aligned} \eta^\dagger(\vec r) &= \mathrm{Re}\eta + i\ \mathrm{Im}\eta = \frac{1}{2}\psi^\dagger_\alpha(\vec r)R_{\alpha\beta}\psi^\dagger_\beta(\vec r), \\ \chi^\dagger_a(\vec r) &= \mathrm{Re}\chi_a + i\ \mathrm{Im}\chi_a = -\frac{i}{2}\psi^\dagger_\alpha(\vec r)(\Gamma^aR)_{\alpha\beta}\psi^\dagger_\beta(\vec r). \end{aligned} \tag{8}$$

The quintet pairing operators $\chi^\dagger_a$ are just the polar combinations of F_z's eigenoperators $P^\dagger_{2,m}$ with the relation

$$P^\dagger_{0,0} = -\frac{\eta^\dagger}{\sqrt{2}}, \quad P^\dagger_{2,\pm2} = \frac{\mp\chi^\dagger_1 + i\chi^\dagger_5}{2}, \quad P^\dagger_{2,\pm1} = \frac{-\chi^\dagger_3 \pm i\chi^\dagger_2}{2}, \quad P^\dagger_{2,0} = -i\frac{\chi^\dagger_4}{\sqrt{2}}. \tag{9}$$

The existence of the R matrix is related to the pseudoreality of $SO(5)$'s spinor representation. It satisfies

$$R^2=-1, \quad R^\dagger=R^{-1}={}^tR=-R, \quad R\Gamma^a R=-{}^t\Gamma^a, \quad R\Gamma^{ab}R={}^t\Gamma^{ab}, \quad (10)$$

where ${}^t\Gamma^{a,ab}$ are the transposed matrices of $\Gamma^{a,ab}$. The anti-unitary time-reversal transformation can be expressed as $T=R\,C$, where C denotes complex conjugation and $T^2=-1$. N, n_a, and L_{ab} transform differently under the T transformation

$$TnT^{-1}=n, \quad Tn_aT^{-1}=n_a, \quad TL_{ab}T^{-1}=-L_{ab}. \quad (11)$$

Under particle-hole transformation, fermions transform as $\psi_\alpha \rightarrow R_{\alpha\beta}\psi^\dagger_\beta, \psi^\dagger_\alpha \rightarrow R_{\alpha\beta}\psi_\beta$. Correspondingly, L_{ab}, n_a transform as

$$\psi^\dagger_\alpha L_{ab,\alpha\beta}\psi_\beta \rightarrow \psi^\dagger_\alpha L_{ab,\alpha\beta}\psi_\beta, \quad \psi^\dagger_\alpha n_{a,\alpha\beta}\psi_\beta \rightarrow -\psi^\dagger_\alpha n_{a,\alpha\beta}\psi_\beta. \quad (12)$$

With the above preparation, the hidden $SO(5)$ symmetry becomes manifest. We can explicitly check all the ten $SO(5)$ generators L_{ab} operators commute with the Hamiltonian Eq. 1 and Eq. 2. In other words, the seven rank-3 spin tensor operators are hidden conserved quantities, which play the same role to the Runge-Lentz vectors in the Hydrogen atom. The kinetic energy parts in Eq. 1 and Eq. 2 have an explicit $SU(4)$ symmetry. The singlet and quintet interactions are proportional to $\eta^\dagger(\vec{r})\eta(\vec{r})$ and $\chi^\dagger_a(\vec{r})\chi_a(\vec{r})$ respectively, thus reducing the symmetry group from $SU(4)$ to $SO(5)$. When $g_0=g_2$ or $U_0=U_2$, the $SU(4)$ symmetry is restored because $\chi^\dagger_a, \eta^\dagger$ together form its 6 dimensional antisymmetric tensor representation. In the continuum model, interactions in other even partial wave channels also keep the $SO(5)$ symmetry. The odd partial wave scattering include spin 1 and 3 channel interactions g_1 and g_3, which together could form the 10-d adjoint representation of $SO(5)$ at $g_1=g_3$. However, to the leading order, p-wave scattering is weak for neutral atoms, and can thus be safely neglected. In the lattice model, this corresponds to the off-site interactions, and can be also be neglected for neutral atoms. The proof of $SO(5)$ invariance in the continuum model applies equally well in the lattice model at any lattice topology and at any filling level. For later convenience, we rewrite the lattice Hamiltonian in the following form:

$$\begin{aligned} H_0 &= -t\sum_{\langle i,j\rangle}\Big\{\psi^\dagger(i)\psi(j)+h.c.\Big\} \\ H_I &= -\sum_{i,1\le a\le 5}\Big\{\frac{V}{2}(n(i)-2)^2+\frac{W}{2}n_a^2(i)\Big\}-(\mu-\mu_0)\sum_i n(i), \end{aligned} \quad (13)$$

with $V=(3U_0+5U_2)/8$ and $W=(U_2-U_0)/2$.

It is natural to think about the symmetry properties in other high fermionic systems with $F=n-\frac{1}{2}$ $(n\ge 3)$. Indeed, we can generalize this $Sp(4)$ symmetry to the $Sp(2n)$ symmetry under certain conditions, but fine tuning is generally speaking needed. In such systems, the s-wave channel interactions can be classified into channels with total spin $S_T=0,2,..,2n-2$ with coupling constants $g_0,g_2,...,g_{2n-2}$, respectively. The $Sp(2n)$ symmetry appears when $g_2=g_4=...=g_{2n-2}$. The proof of the $Sp(2n)$ symmetry and an introduction to the $Sp(2n)$ algebra are given in Ref. [23].

2.3. *The SO(8) structure in the bipartite lattice systems*

We next further explore the full symmetry of the spin-3/2 system by extending the above algebra to include the *p*-*p* channel. In spin-1/2 bipartite lattice systems, it is well known that the particle density and η-pairing operators form a pseudospin $SU(2)$ algebra [47]. For spin-3/2 systems, we embed the above $SO(5)$ algebra inside the $SO(8)$ algebra involving both *p*-*h* and *p*-*p* channels. $SO(8)$ is the largest Lie algebra which can be constructed with four component fermions. The $SO(8)$ symmetry is shown to be dynamically generated in spin-$\frac{1}{2}$ two-leg ladder systems, and its effect was extensively studied [48,49]. The $SO(8)$ algebra here is attributed with different physical meaning. Its generators M_{ab} $(0 \le a < b \le 7)$ reads

$$M_{ab} = \begin{pmatrix} 0\ \mathrm{Re}\chi_1 & \sim & \mathrm{Re}\chi_5 & N & \mathrm{Re}\eta \\ & & & \mathrm{Im}\chi_1 & n_1 \\ & L_{ab} & & \sim & \sim \\ & & & \mathrm{Im}\chi_5 & n_5 \\ & & & 0 & -\mathrm{Im}\eta \\ & & & & 0 \end{pmatrix},$$

with $N = (n-2)/2$. In the bipartite lattice, we define the global $SO(8)$ generators as $M_{ab} = \sum_i M_{ab}(i)$ for $M_{ab} = n, n_a, L_{ab}$ in the *p*-*h* channel, and $M_{ab} = \sum_i (-)^i M_{ab}(i)$ for $M_{ab} = \mathrm{Re}\eta, \mathrm{Im}\eta, \mathrm{Re}\chi_a, \mathrm{Im}\chi_a$ in the *p*-*p* channel.

At $U_0 = 5\ U_2$ and $\mu = \mu_0$ $(\mu_0 = \frac{U_0+5U_2}{4})$, the three spin singlet sets of $E_{1,4,6}$ become degenerate. They form a spin-1 representation for the $SU(2)$ algebra spanned by $\eta^\dagger, \eta, N$. In this case, H_I can be rewritten as

$$H_I = \sum_{i, 1 \le a, b \le 5} \{-U_2\ L^2_{ab}(i) - (\mu - \mu_0) n(i)\}, \tag{14}$$

by using the Fierz identity $\sum_{1 \le a \le 5} L^2_{ab}(i) + \sum_{1 \le a \le 5} n^2_a(i) + 5N^2(i) = 5$. The symmetry at half-filling is $SO(5) \otimes SU(2)$, which unifies the charge density wave (CDW) and the singlet pairing (SP) order parameters. Away from half-filling, this symmetry is broken but $\eta, \eta^\dagger$ are still eigen-operators since $[H, \eta^\dagger] = -(\mu - \mu_0)\eta^\dagger$, and $[H, \eta] = (\mu - \mu_0)\eta$.

Similarly, at $U_0 = -3U_2$ and $\mu = \mu_0$, the two spin singlet states $E_{1,6}$ and the spin quintet states E_3 become degenerate. They form a 7-vector representation for the $SO(7)$ group spanned by $M_{ab} (0 \le a < b \le 6)$. The H_I can be reorganized into

$$H_I = \sum_{i, 0 \le a < b \le 6} \Big\{ \frac{2}{3} U_2\ M_{ab}(i)^2 - (\mu - \mu_0) n(i) \Big\}. \tag{15}$$

The $SO(7)$ symmetry is exact at half-filling. Its 7-d vector representation unifies the order parameters of the staggered $\sum_i (-)^i n_a(i)$, and the singlet pairing

$\sum_i \eta^\dagger(i)$. Its 21-d adjoint representation unifies the order parameters of the staggered $\sum_i(-)^i L_{ab}(i)$, the CDW $\sum_i(-)^i N(i)$, and quintet pairing $\sum_i \chi^\dagger(i)$. Away from half-filling, quintet pairing operators are spin 2 quasi-Goldstone operators $[H, \chi_a^\dagger(\chi_a)] = \mp(\mu - \mu_0)\chi_a^\dagger(\chi_a)$. These χ-modes are just the analogs of the π modes in the high T$_c$ context[22].

3. Effects of the $SO(5)$ symmetry

In this section, we review the $SO(5)$ effect to the Fermi liquid theory [21], the mean field phase diagram [21], the sign problem in quantum Monte-Carlo simulations [21,23]. We also construct effective strong coupling models at half-filling in Sect. 3.3.

3.1. *The $SO(5)$ Fermi liquid theory*

The Fermi liquid theory in spin 3/2 systems is simplified by the $SO(5)$ symmetry. A particle-hole pair in such systems can carry total spins with $S_T = 0, 1, 2, 3$, thus it generally requires four Fermi liquid functions in these channels. However, the $SO(5)$ symmetry reduces them to three independent sets as

$$f_{\alpha\beta,\gamma\delta}(\vec{p}, \vec{p}') = f_s(\vec{p}, \vec{p}') + f_v(\vec{p}, \vec{p}')(\frac{\Gamma^a}{2})_{\alpha\beta}(\frac{\Gamma^a}{2})_{\gamma\delta} + f_t(\vec{p}, \vec{p}')(\frac{\Gamma^{ab}}{2})_{\alpha\beta}(\frac{\Gamma^{ab}}{2})_{\gamma\delta}, \quad (16)$$

where $\vec{p}$ and $\vec{p}\prime$ are the momenta of two particles near the Fermi surface, $f_{s,v,t}$ describe the interaction in the $SO(5)$ scalar, vector, and tensor channels, respectively. Within the s-wave scattering approximation, these functions become constants as $f_s = (g_0 + 5g_2)/16$, $f_v = (g_0 - 3g_2)/4$, $f_t = -(g_0 + g_2)/4$. In other words, the two channels of $S_T = 1, 3$ are degenerate and included in the tensor channel. The susceptibility in each channel reads $\chi_{s,v,t}(\vec{r} - \vec{r}', t - t') = -i\theta(t - t')\langle|[\hat{O}_{s,v,t}(\vec{r}, t), \hat{O}_{s,v,t}(\vec{r}', t')]|\rangle$ with $\hat{O}_{s,v,t} = n$, n_a, L_{ab}, respectively. Within the random-phase approximation, the Fourier transforms in the momentum and frequency space are $\chi_{s,v,t}(q, \omega) = \chi^0(q, \omega)/[1 + f_{s,v,t}\chi^0(q, \omega)]$, where $\chi^0(q, \omega)$ is the standard Lindhard function of the free systems. The degeneracy in the spin 1 and 3 channels was first pointed out in Ref. [20], but it appears accidentally there. It is actually exact and protected by the generic $SO(5)$ symmetry. Experiments in the Fermi liquid regime can determine the four Fermi liquid constants in the $S_T = 0, 1, 2, 3$ channels separately and verify the degeneracy between spin 1 and 3 channels.

3.2. *Mean field analysis at half-filling in bipartite lattices*

In the weak coupling limit, we perform a mean-field analysis to the lattice Hamiltonian Eq. 2 at half-filling in a bipartite lattice. The decoupling is performed in all

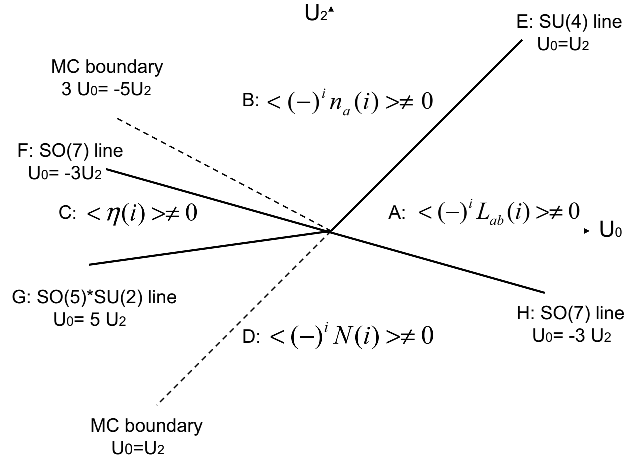

Fig. 2. The MF phase diagram at half-filling in a bipartite lattice. A) and B): staggered phases of the $SO(5)$ adjoint and vector Reps; C): the singlet superconductivity; D): CDW; E), F), G) and H): exact phase boundaries with higher symmetries. Between the dashed lines ($U_0 \leq U_2 \leq -3/5U_0$) , a Monte-Carlo algorithm free of the sign problem is possible. From Wu *et al.* Ref. [21].

of the direct, exchange, and pairing channels as

$$\begin{aligned}
H_{MF} = & -t \sum_{\langle ij,\sigma\rangle} \Big\{ c^\dagger_{i,\sigma} c_{j,\sigma} + h.c. \Big\} - (\mu - \mu_0) \sum_{i,\sigma} n(i) - \frac{3U_2 - U_0}{2} \sum_{i, 1\leq a \leq 5} \langle n_a(i) \rangle n_a(i) \\
& - \frac{U_0 + U_2}{2} \sum_{i, 1\leq a < b \leq 5} \langle L_{ab}(i) \rangle L_{ab}(i) + \frac{U_0 + 5U_2}{2} \sum_i \langle N(i) \rangle N(i) \\
& + U_0 \sum_i \Big\{ \langle \mathrm{Re}\eta(i) \rangle \ \mathrm{Re}\eta(i) + \langle \mathrm{Im}\eta(i) \rangle \ \mathrm{Im}\eta(i) \Big\} + U_2 \sum_{i, 1\leq a\leq 5} \Big\{ \langle \mathrm{Re}\chi_a(i) \rangle \mathrm{Re}\chi_a(i) \\
& + \langle \mathrm{Im}\chi_a(i) \rangle \mathrm{Im}\chi_a(i) \Big\} \qquad (17)
\end{aligned}$$

We solve the Eq. 17 self-consistently at half-filling in the 2D square lattice with the phase diagram depicted in Fig. 2. We use the following MF ansatz:

$$\begin{aligned}
&\langle n_a(i) \rangle = (-)^i \overline{n}_a, \quad \langle N(i) \rangle = (-)^i \overline{N}, \quad \langle L_{ab}(i) \rangle = (-)^i \overline{L}_{ab} \\
&\langle \eta(i) \rangle = \overline{\eta}, \qquad\quad \langle \chi_a(i) \rangle = \overline{\chi}_a. \qquad (18)
\end{aligned}$$

There are four phases A, B, C and D with bulk area separated by high symmetry lines E, F, G and H. In phase A, the staggered order parameters $\langle (-)^i L_{ab}(i) \neq 0 \rangle$ form $SO(5)$'s adjoint representation (Rep) with the residue symmetry $SO(3) \otimes SO(2)$, thus the Goldstone (GS) manifold is $SO(5)/[SO(3) \otimes SO(2)]$. In phase B, the staggered order parameters $\langle (-)^i n^a(i) \rangle \neq 0$ form $SO(5)$'s vector Rep with

Phase	order parameters	GS manifold	GS modes
A	$(-)^i L_{ab}(i)$	$SO(5)/[SO(3) \otimes SO(2)]$	6
B	$(-)^i n_a(i)$	$SO(5)/SO(4) \equiv S^4$	4
C	$\eta(i)$	$U(1)$	1
D	CDW	/	/
E	$(-)^i n_a(i), (-)^i L_{ab}(i)$	$U(4)/[U(2) \otimes U(2)]$	8
F	$(-)^i n_a(i), \eta(i)$	$SO(7)/SO(6) \equiv S^6$	6
G	CDW, $\eta(i)$	$SO(3)/SO(2) \equiv S^2$	2
H	CDW, $\chi_a(i), (-)^i L_{ab}(i)$	$SO(7)/[SO(5) \times SO(2)]$	10

Table 1. Order parameters, the corresponding Goldstone manifolds and the number of Goldstone modes in each phase on the bipartite lattice at half-filling. From Wu *et al.* Ref. [21].

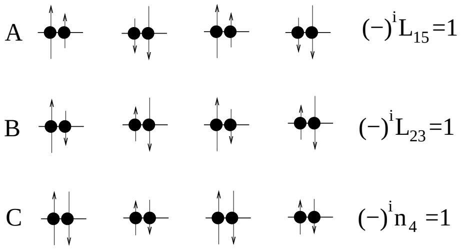

Fig. 3. Three configurations of classical Neel states on the $SU(4)$ line.

the residue symmetry $SO(4)$ and the GS manifold S^4. In phase C and D, order parameters are the singlet superconductivity $\langle \eta(i) \rangle \neq 0$ and charge density wave (CDW) $\langle (-)^i N(i) \rangle \neq 0$ respectively, where the $SO(5)$ symmetry is unbroken. $SU(4)$ symmetry arises at line E where the staggered order parameters $(-)^i L_{ab}(i)$ and $(-)^i n^a(i)$ become degenerate with GS manifold $U(4)/[U(2) \otimes U(2)]$. Line F and H are characterized by the $SO(7)$ symmetry. On the line F, order parameters $(-)^i n^a(i)$ and $\eta(i)$ are degenerate with the GS manifold S^6. One the line E, order parameters $(-)^i L_{ab}(i)$, CDW and $\chi^a(i)$ are degenerate with the GS manifold $SO(7)/[SO(5) \otimes SO(2)$. The $SO(5) \otimes SU(2)$ symmetry arises at line G, where CDW and singlet pairing become degenerate. Order parameters in each phase and corresponding GS modes are summarized in Table 3.1.

3.3. *Strong coupling modes at half-filling*

Next we construct the effect Hamiltonians for the bosonic sector in the strong coupling limit. Around the $SU(4)$ line E with $U_0 = U_2 = U$, the low energy states are the six states with double occupancy $E_{3,4}$. The exchange model in this projected

Hilbert space reads

$$H_{eff} = J_L \sum_{1 \le a < b \le 5} L_{ab}(i) L_{ab}(j) + J_n \sum_{1 \le a \le 5} n_a(i) n_a(j) + \frac{\Delta U_1}{4} \sum_{i, 1 \le a < b \le 5} L^2_{ab}(i), \quad (19)$$

with $\Delta U_1 = U_2 - U_0$. Along the $SU(4)$ line, $\Delta U_1 = 0$ and $J_L = J_n = 4\frac{t^2}{U}$, Eq. 19 is just the $SU(4)$ Heisenberg model with each site in the 6-d representation. At three dimensions, we expect the ground state to be long range Neel ordered. Three possible classical configurations A, B, C are shown in Fig. 3, which can be rotated into each other under $SU(4)$ operations. They are eigenstates of three $SU(4)$ Cartan generators: $L_{23} = \frac{1}{2}(n_{\frac{3}{2}} - n_{\frac{1}{2}} + n_{\frac{-1}{2}} - n_{\frac{-3}{2}})$, $L_{15} = \frac{1}{2}(n_{\frac{3}{2}} + n_{\frac{1}{2}} - n_{\frac{-1}{2}} - n_{\frac{-3}{2}})$, and $n_4 = \frac{1}{2}(n_{\frac{3}{2}} - n_{\frac{1}{2}} - n_{\frac{-1}{2}} + n_{\frac{-3}{2}})$. A nonzero onsite ΔU_1 term reduces the symmetry down to $SO(5)$ and brings the difference between J_L and J_n. The latter contribution is at the order of $(t/U)^2$ compared to the former, thus is less important. In phase A, five quintet states become the lowest energy states, then the J_n and ΔU_1 terms can be neglected, and thus Eq. 19 reduces to the $SO(5)$ Heisenberg model. The Neel states in phase A can be represented in Fig. 3 A and B which breaks TR symmetry. In phase B, the singlet state becomes the lowest energy state, Eq. 3 reduces to the $SO(5)$ rotor model whose (spin-nematic) Neel order keeps the TR symmetry as represented in Fig. 3 C. A transition from a site singlet phase to the Neel ordered phase happens at $zJ_1 \approx \Delta U_1$ where z is the coordination number.

Next we look at the $SO(7)$ line F where the lowest energy state is the singlet state E_4, and the next bosonic states are the 7-fold degenerate sets of $E_{0,3,6}$. In phase B or C , $E_{0,6}$ becomes higher or lower than E_3, respectively. An anisotropic $SO(7)$ rotor model can be constructed to describe the above effect:

$$\begin{aligned} H_{eff,2} = {} & J_n \sum_{1 \le a \le 5} n_a(i) n_a(j) - \frac{J_\eta}{2} \{ \eta^\dagger(i) \eta(j) + \eta(i) \eta^\dagger(j) \} \\ & + \frac{\Delta U_2}{2} \sum_{0 \le a < b \le 6} M^2_{ab}(i) + \frac{\Delta U_3}{2} N^2(i), \end{aligned} \quad (20)$$

where $\Delta U_2 = \frac{U_2 - U_0}{6}$ and $\Delta U_3 = \frac{U_0 + 3U_2}{2}$. Along line F, $\Delta U_3 = 0$ and $J_n = J_\eta$, thus the antiferromagnetic spin-nematic order and singlet superconductivity become degenerate. This $SO(7)$ symmetry is the generalization of the $SO(5)$ theory of high T_c superconductivity [22]. In phase C, $\Delta U_3 < 0$, the staggered spin-nematic order n_a is disfavored, and Eq. 20 reduces to the $U(1)$ rotor model for the singlet superfluidity. On the other hand, for $\Delta U_3 > 0$ in phase B, Eq. 20 reduces to the $SO(5)$ rotor model for n_a.

Along line G and in phases C and D, the lowest energy states are three $SO(5)$ singlets of $E_{1,4,6}$ which form a spin-1 Rep for the pseudospin $SU(2)$ algebra. The effective model is anisotropic spin-1 Heisenberg-like as

$$H_{eff,3} = \frac{-J_\eta}{2} \{ \eta^\dagger(i) \eta(j) + \eta(i) \eta^\dagger(j) \} + J_n N(i) N(j) + \Delta U_4 N^2(i), \quad (21)$$

with $\Delta U_4 = \frac{-U_0+5U_2}{2}$. Along the $SO(5)\otimes SU(2)$ line G, $J_\eta = J_n = \frac{2t^2}{|U_0|}$ and $\Delta U_4 = 0$, the singlet superfluidity and CDW are degenerate. In the phase C where $\Delta U_4 > 0$, Eq. 21 reduces into the $U(1)$ rotor model for superfluidity, while in the phase D where $\Delta U_4 < 0$, Eq. 21 reduces into the Ising model for CDW.

Similarly, around the other $SO(7)$ line H, the sets of $E_{1,4,6}$ consist the low energy Hilbert space. We can construct the anisotropic $SO(7)$ Heisenberg model in the 7-vector representation as

$$\begin{aligned} H_{eff} &= J_L \sum_{1\le a<b\le 5} L_{ab}(i)L_{ab}(j) - \frac{J_\chi}{2}\sum_{1\le a\le 5}\left\{\chi^\dagger_a(i)\chi_a(j) + \chi_a(i)\chi^\dagger_a(j)\right\} \\ &\quad + J_N N(i)N(j) + \Delta U_5 \sum_{i,1\le a<b\le 5} N^2(i), \end{aligned} \tag{22}$$

where $J_L = J_\chi = J_N = \frac{4t^2}{U_0+U_2}$ and $\Delta U_5 = 0$ around line H. In phase A where $\Delta U_5 > 0$, Eq. 22 reduces into the $SO(5)$ Heisenberg model, while in phase B where $\Delta U_5 < 0$, it reduces into the Ising model for the CDW order.

3.4. *Quantum Monte-Carlo sign problem in spin-3/2 systems*

The sign problem is a major difficulty for the quantum Monte-Carlo (QMC) simulations to apply to fermionic systems. In spin-3/2 systems, due to the structure of $SO(5)$ algebra, the sign problem in the the auxiliary field QMC [50] is shown to be absent in a large part of the phase diagram [21,51,23].

We use the equivalent version of the lattice Hamiltonian Eq. 13 where interactions are represented in terms of the TR even operators n and n_a. By using the Hubbard-Stratonovich (H-S) transformation, the four-fermion interactions of n^2 and n_a^2 are decoupled at $V, W > 0$ (or $-3/5\ U_0 > U_2 > U_0$), and the resulting partition function can be written as

$$Z = \exp\Big\{ -V\int_0^\beta d\tau \sum_i (n(i,\tau)-2)^2 - W\int_0^\beta d\tau \sum_{i,a} n_a^2(i,\tau)\Big\}\,\det\Big\{I+B\Big\}. \tag{23}$$

The functional determinant $I + B = I + \mathcal{T} e^{-\int_0^\beta d\tau H_K + H_i(\tau)}$ is from the integration of fermion fields, n and n_a are real H-S bose fields. The kinetic energy H_K and time-dependent decoupled interaction $H_i(\tau)$ read

$$\begin{aligned} H_K &= -t\sum_i(\psi^\dagger_{i,\sigma}\psi_{j,\sigma} + h.c.) - \sum_i(\mu-\mu_0)\psi^\dagger_{i\sigma}\psi_{i\sigma} \\ H_{int}(\tau) &= -V\sum_i \psi_{i,\sigma}(\tau)\psi_{i,\sigma}(\tau)n(i,\tau) - W\sum_{i,a}\psi^\dagger_{i,\sigma}(\tau)\Gamma^a_{\sigma,\sigma'}\psi_{i,\sigma'}(\tau)n_a(i,\tau). \end{aligned} \tag{24}$$

Generally speaking, $\det(I+B)$ may not be positive definite, making it difficult to use the probability interpretation of the functional integrand in the QMC simulation. However, if the above decoupling scheme satisfies an TR-like symmetry, the following theorem states the positivity of $\det(I+B)$ [52,53,23]: if there exists an anti-unitary operator T, such that

$$TH_KT^{-1} = H_K, \quad TH_IT^{-1} = H_I, \quad T^2 = -1, \tag{25}$$

then the eigenvalues of the $I+B$ matrix always appear in complex conjugate pairs no matter $I+B$ is diagonalizable or not, *i.e.*, if λ_i is an eigenvalue, then λ_i^* is also an eigenvalue. If λ_i is real, it is two-fold degenerate. In this case, the fermion determinant is positive definite,

$$\det(I+B) = \prod_i |\lambda_i|^2 \geq 0. \tag{26}$$

The detailed proof can be found in Ref. [23]. The T operator does not need to be the physical TR operator. As long as Eq. 25 is satisfied, the positivity of $\det(I+B)$ is guaranteed. We emphasis that the above criterion applies for any lattice geometry and doping levels.

Because both the density n and spin-nematic operators n_a are TR even operators, the sign problem disappears as long as $V, W > 0$ or $-3/5\ U_0 > U_2 > U_0$ (see Fig. 2). This region includes interesting competing orders such as the staggered spin-nematic order n_a, singlet superfluidity η, CDW, and also the phase boundaries of the $SO(7)$ line F and the $SO(5)\otimes SU(2)$ line G. The absence of the sign problem provide a good opportunity to study the competition among these orders, in particular, then doping effect, the frustration on the triangular lattice, *etc*, which are difficult at low temperatures for previous Monte-Carlo works.

The above sign problem criterion can also be applied to other systems, such as multi-band Hubbard models. For example, Capponi *et al.* showed a ground state staggered current order by QMC simulations without the sign problem in a bi-layer extended Hubbard model [51].

4. Quintet Cooper pairing and half-quantum vortices

When the interaction constant in the quintet channel g_2 goes negative, spin 3/2 systems can support quintet Cooper pairing, i.e., Cooper pairs with total spin 2. In this section, we discuss the collective modes in this state, and the topological defect of half-quantum vortex and related non-Abelian Cheshire charges [24].

4.1. *Collective modes in the quintet pairing states*

We write the BCS mean field Hamiltonian for the quintet Cooper pairing state as

$$\begin{aligned} H_{MF} = \int d^D r \Big\{ &\sum_{\alpha=\pm\frac{3}{2},\pm\frac{1}{2}} \psi_\alpha^\dagger(r)\big(\frac{-\hbar^2\nabla^2}{2M} - \mu\big)\psi_\alpha(r) + \sum_{a=1\sim5} \chi_a^\dagger(r)\Delta_a(r) + h.c. \\ &- \frac{1}{g_2}\Delta_a^*(r)\Delta_a(r)\Big\}. \end{aligned} \tag{27}$$

Δ_a is proportional to the ground state expectation value of the quintet pairing operators χ_a by $\Delta_a(r) = g_2 \langle \chi^\dagger_a(r) \rangle$ $(a = 1 \sim 5)$. The five χ_a operators defined in Eq. 8 are the spin channel counterparts of the five atomic d-orbitals $(d_{xy}, d_{xz}, d_{yz}, d_{3z^2-r^2}, d_{x^2-y^2})$. They transform as a 5-vector under the $SO(5)$ group.

The Ginzburg-Landau (GL) free energy around T_c for the quintet pairing was studied in Ref. [45] without noticing the hidden $SO(5)$ symmetry. Facilitated by this high symmetry, we organize the GL free energy in an explicitly $SO(5)$ invariant way, and give a general analysis to the quintet pairing structures. The GL free energy reads

$$F_{GL} = \int d^D r \;\; \gamma \nabla \Delta^*_a \nabla \Delta_a + \alpha(T) \Delta^*_a \Delta_a + \frac{\beta_1}{2} |\Delta^*_a \Delta_a|^2 + \frac{\beta_2}{2} \sum_{a<b} |\frac{\Delta^*_a \Delta_b - \Delta^*_b \Delta_a}{\sqrt{2}}|^2,$$

$$\alpha = -\frac{1}{2}\frac{dn}{d\epsilon}(1 - \frac{T}{T_c}), \quad \beta_1 = \beta_2 = \frac{1}{2}\frac{dn}{d\epsilon}\frac{7\zeta(3)}{8\pi^2 T_c^2}, \quad \gamma = \frac{n\hbar^2}{4M}\frac{7\zeta(3)}{8\pi^2 T_c^2}. \qquad (28)$$

where n is the particle density, $dn/d\epsilon$ is the density of states at the Fermi level, and $\zeta(x)$ is the Riemann zeta function. At $\beta_2 > 0$ or $\beta_2 < 0$, two different pairing states are favorable to minimize the free energy, i.e., the unitary polar state and non-unitary ferromagnetic state respectively. The polar state is parameterized as $\Delta_a = |\Delta(T)| e^{i\theta} d_a$, where θ is the $U(1)$ phase, and $\hat{d} = d_a \hat{e}_a$ is a 5-d unit vector in the internal spin space. The ferromagnetic pairing state is described as $\Delta_a = |\Delta(T)| e^{i\theta}(d_{1a} + i\ d_{2a})$ with $\hat{d}_1$, $\hat{d}_2$ two orthogonal 5-d unit vectors. The standard Gor'kov expansion gives $\beta_2 > 0$, thus the polar state is stable in the framework of the BCS theory. In the following, we focus on the polar state which is also expected to be stable at zero temperature.

At $T = 0K$, various low energy dissipationless Goldstone modes exist due to the broken symmetries. In addition to the usual phonon mode, four branches of spin wave modes carrying $S = 2$ arise from the breaking of the $SO(5)$ symmetry down to $SO(4)$. The above GL free energy constructed around T_c does not apply to describe these Goldstone modes. For this purpose, Cooper pairs can be treated as composite bosons. This treatment gives a good description of the phonon mode in the neutral singlet BCS superfluid in Ref. [54,55]. Here, we generalize it to the quintet pairing by considering a phenomenological Hamiltonian for spin 2 bosons

$$H_{eff} = \int d^D r \; \frac{\hbar^2}{4M} \sum_a |\nabla \Psi_a|^2 + \frac{1}{2\chi_\rho}(\Psi^*_a \Psi_a - \rho_0)^2 + \frac{1}{2\chi_{sp}} \sum_{a<b} (\Psi^*_c L^{ab}_{cd} \Psi_d)^2, \quad (29)$$

where Ψ_as are the boson operators in the polar basis, $L^{ab}_{cd} = i(\delta_{ac}\delta_{bd} - \delta_{ad}\delta_{bc})$ are the $SO(5)$ generators in the 5×5 representation, the equilibrium Cooper pair density ρ_0 is half of the particle density ρ_f, χ_ρ and χ_{sp} are proportional to the compressibility and $SO(5)$ spin susceptibility respectively. Taking into account the Fermi liquid correction, $\chi_\rho = N_f/[4(1+F^s_0)]$ and $\chi_{sp} = N_f/[4(1+F^t_0)]$, where N_f is the fermion density of states at the Fermi energy, $F^{s,t}_0$ are the Landau parameters defined in the $SO(5)$ scalar and tensor channels [21] respectively. We introduce $\rho(r)$ and $l_{ab}(r)$ as the Cooper pair density and $SO(5)$ spin density respectively, and parameterize

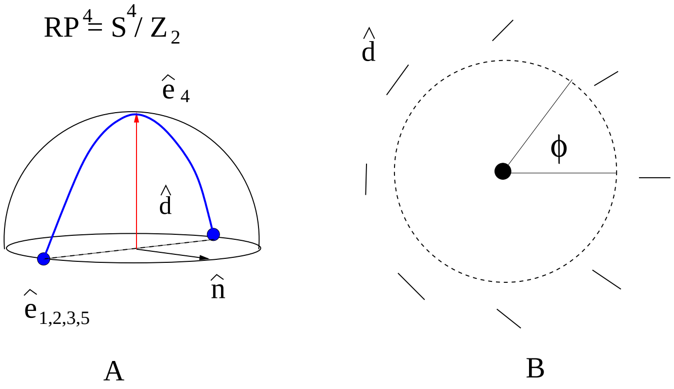

Fig. 4. A) The Goldstone manifold of $\hat{d}$ is a 5D hemisphere RP^4. It contains a class of non-contractible loops as marked by the solid curve. B) The π-disclination of $\hat{d}$ as a HQV. Assume that $\hat{d} \parallel \hat{e}_4$ at $\phi = 0$. As the azimuthal angle ϕ goes from 0 to 2π, $\hat{d}$ is rotated at the angle of $\phi/2$ around any axis $\hat{n}$ in the S^3 equator spanned by $\hat{e}_{1,2,3,5}$. From Wu *et al.* Ref. [24].

$\Psi_a = \sqrt{\rho_0} e^{i\theta} d_a$. Using the standard commutation rules between ρ and θ, l_{ab} and $\hat{d}_a$, we arrive at

$$\chi_\rho \partial_t^2 \theta - \frac{\hbar^2 \rho_s}{2M} \nabla^2 \theta = 0, \tag{30}$$

$$\partial_t l_{ab} = \frac{\hbar^2 \rho_{sp}}{2M} (d_a \nabla^2 d_b - d_b \nabla^2 d_a), \quad \chi_{sp} \partial_t d_a = -l_{ab} d_b, \tag{31}$$

where ρ_s and ρ_{sp} are the superfluid density and spin superfluid density respectively. At $T = 0K$ in a Galilean invariant system, ρ_s is just $\rho_f/2$, while ρ_{sp} receives Fermi liquid corrections as $\rho_{sp}/\rho_s = (1 + F_1^v/3)/(1 + F_1^s/3)$ [56] where F_1^v is the Landau parameter in the $SO(5)$ vector channel [21]. The sound and spin wave velocities are obtained as $v_s = \sqrt{\rho_0/(2\chi_\rho M)}$ and $v_{sp} = \sqrt{\rho_0/(2\chi_{sp} M)}$, respectively.

4.2. *Half-quantum vortex*

Superfluids with internal structure can support half-quantum vortex (HQV) as a stable topological defect because the order parameter contains a Z_2 gauge symmetry. For the quintet pairing case, $\Delta_a = |\Delta| e^{i\theta} \hat{d}_a$ is invariant under the combined operation

$$\hat{d} \to -\hat{d}, \quad \theta \to \theta + \pi. \tag{32}$$

As a result, $\hat{d}$ is actually a directionless director instead of a true vector. Thus the fundamental group of the GS manifold is $\pi_1(RP^4 \otimes U(1)) = Z \otimes Z_2$ as depicted in Fig. 4 A. The Z_2 feature gives rise to the existence of HQV as depicted in Fig. 4 B. As we move along a loop enclosing HQV, the π phase mismatch in the θ field is offset by a π-disclination in the $\hat{d}$-field, thus Δ_a's are still single-valued.

Next we check the energetics of HQV. The static energy function can be written as

$$E=\int d^D r \frac{\hbar^2}{4M}\Big\{\rho_s(\nabla\theta)^2+\rho_{sp}(\nabla\hat{d})^2\Big\}. \tag{33}$$

The energy density per unit length of a single quantum vortex is $E_1=\frac{\hbar^2}{4M}\rho_s\log\frac{L}{a}$, while that of two isolated HQVs is $E_2=\frac{\hbar^2}{8M}(\rho_s+\rho_{sp})\log\frac{L}{a}$. Thus for $\rho_{sp}<\rho_s$, a single quantum vortex is energetically less favorable than a pair of HQVs. Although at the bare level $\rho_s=\rho_{sp}$, ρ_{sp} receives considerable Fermi liquid correction and strong reduction due to quantum fluctuations in the 5D internal space. Generally speaking, $\rho_{sp}<\rho_s$ holds in terms of their renormalized values.

An interesting property of the HQV is its Alice string behavior [57,58]. In this context, it means that a quasi-particle change its spin quantum numbers after it adiabatically encircles the HQV. For example, in the ^{3}He-A phase, a quasi-particle with spin ↑ changes to ↓ up to a $U(1)$ Berry phase. The HQV in the quintet pairing case behaves as a non-Abelian generalization of the above effect. Without loss of generality, we assume that $\hat{d}\parallel\hat{e}_4$ at the azimuthal angle $\phi=0$. As ϕ changes from 0 to 2π, $\hat{d}$ is rotated at the angle of $\phi/2$ in the plane spanned by $\hat{e}_4$ and $\hat{n}$, where $\hat{n}$ is a unit vector perpendicular to $\hat{e}_4$, i.e., a vector located in the S^3 sphere spanned by $\hat{e}_{1,2,3,5}$. We define such a rotation operation as $U(\hat{n},\phi/2)$. When U acts on an $SO(5)$ spinor, it takes the form of $U(\hat{n},\phi/2)=\exp\{-i\frac{\phi}{2}\frac{n_b\Gamma^{b4}}{2}\}$, when U acts on an $SO(5)$ vector, it behaves as $U(\hat{n},\phi/2)=\exp\{-i\frac{\phi}{2}n_bL^{b4}\}$ where L^{ab}'s are the $SO(5)$ generators in the 5×5 vector representation. The resulting configuration of $\hat{d}$ is $\hat{d}(\hat{n},\phi)=U(\hat{n},\phi/2)\hat{d}(\hat{n},0)=(\cos\frac{\phi}{2}\hat{e}_4-\sin\frac{\phi}{2}\hat{n})$. As fermionic quasi-particles circumscribe around the vortex line adiabatically, at $\phi=2\pi$ fermions with $S_z=\pm\frac{3}{2}$ are rotated into $S_z=\pm\frac{1}{2}$ and *vice versa*. For convenience, we change the basis Ψ for the fermion wavefunction to $(|\frac{3}{2}\rangle,|-\frac{3}{2}\rangle,|\frac{1}{2}\rangle,|-\frac{1}{2}\rangle)^T$. After taking into account the π phase of the superfluid vortex, Ψ transforms by

$$\Psi_a\rightarrow\Psi^\prime_a=iU(\hat{n},\pi)_{\alpha\beta}\Psi_\beta=\begin{pmatrix}0 & W\\ W^\dagger & 0\end{pmatrix}_{\alpha\beta}\Psi_\beta \tag{34}$$

where W is an $SU(2)$ phase depending on the direction of $\hat{n}$ on the S^3 sphere as

$$W(\hat{n})=\begin{pmatrix}n_3+in_2 & -n_1-in_5\\ n_1-in_5 & n_3-in_2\end{pmatrix}. \tag{35}$$

The non-conservation of spin in this adiabatic process is not surprising because the $SO(5)$ symmetry is completely broken in the configuration depicted in Fig. 4 B.

4.3. *SO*(4) *Cheshire charge*

Another interesting concept related to the Alice string in the gauge theory is the Cheshire charge, which means a HQV pair or loop can carry spin quantum number. When a quasi-particle carrying spin penetrate the HQV loop or pair, the spin

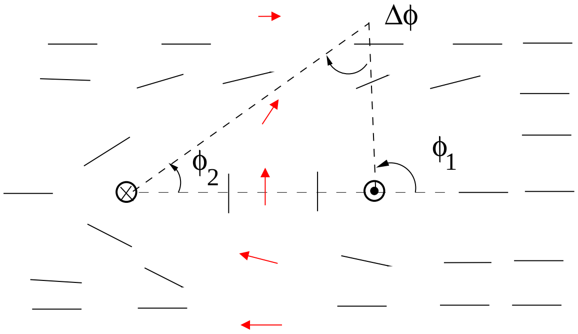

Fig. 5. The configuration of a π-disclination pair or loop described by Eq. 37. $\phi_{1,2}$ and $\Delta\phi$ are azimuthal angles and $\hat{d}(\vec{r}) \parallel \hat{e}_4$ as $\vec{r} \to \infty$. After a fermion passes the HQV loop, the components with $S_z = \pm\frac{3}{2}$ change to $S_z = \pm\frac{1}{2}$ and *vice versa* with an $SU(2)$ matrix defined in Eq. 34. From Wu *et al.* Ref. [24].

conservation is maintain by exciting the Cheshire charge of the HQV loop or pair. Below we will construct the $SO(4)$ Cheshire charge in the quintet Cooper pairing state.

We begin with a uniform ground state where $\hat{d}$ is parallel to $\hat{e}_4$ axis where the $SO(4)$ symmetry generated by $\Gamma_{ab}(a, b = 1, 2, 3, 5)$ is preserved. This $SO(4)$ algebra can be reorganized into two inter-commutable $SU(2)$ algebras as

$$\begin{aligned} T_1(T_1') &= \frac{1}{4}(\pm\Gamma_{35} - \Gamma_{12}), \quad T_2(T_2') = \frac{1}{4}(\pm\Gamma_{31} - \Gamma_{25}), \\ T_3(T_3') &= \frac{1}{4}(\pm\Gamma_{23} - \Gamma_{15}). \end{aligned} \tag{36}$$

$T_{1,2,3}$ and $T'_{1,2,3}$ act in the subspaces spanned by $|\pm\frac{3}{2}\rangle$ and $|\pm\frac{1}{2}\rangle$, respectively. $SO(4)$ representations are denoted by $|T, T_3; T', T_3'\rangle$, i.e., the direct-product of representations of two $SU(2)$ groups.

Now we construct a HQV loop or pair as depicted in Fig. 5. where $\phi_{1,2}$ are azimuthal angles respect to the vortex and anti-vortex cores respectively. The solution of the configuration of the $\hat{d}$ vector is described by the difference between two azimuthal angles $\Delta\phi = \phi_2 - \phi_1$ as

$$\hat{d}(\hat{n}, \Delta\phi) = \cos\frac{\Delta\phi}{2}\hat{e}_4 - \sin\frac{\Delta\phi}{2}\hat{n}, \tag{37}$$

where $\hat{n}$ again is a unit vector on the S^3 equator. This configuration is called a phase-sharp state denoted as $|\hat{n}\rangle_{vt}$. Because the above $SO(4)$ symmetry is only broken within a small region around the HQV loop, quantum fluctuations of $\hat{n}$ dynamically restore the $SO(4)$ symmetry as described by the Hamiltonian

$$H_{rot} = \sum_{a,b=1,2,3,5} \frac{M_{ab}^2}{2I}, \quad M_{ab} = i(\hat{n}_a\partial_{\hat{n}_b} - \hat{n}_b\partial_{\hat{n}_a}), \tag{38}$$

with the moment of inertial $I = \chi_{sp} \int d^D r \; \rho_0 \sin^2 \frac{\Delta\phi}{2}$. Thus the zero modes $|\hat{n}\rangle_{vort}$ are quantized into the global $SO(4)$ Cheshire charge state, which is a non-Abelian generalization of the $U(1)$ Cheshire charge in the ^{3}He-A phase [59]. The Cheshire charge density is localized around the vortex loop. In contrast, the Cheshire charge in the gauge theory is non-localized [57,58]. The HQV loop in the $SO(4)$ Cheshire charge eigenstates are defined as $|TT_3; T'T'_3\rangle_{vt} = \int_{\hat{n}\in S^3} d\hat{n} \; F_{TT_3;T'T'_3}(\hat{n}) \; |\hat{n}\rangle_{vt}$, where $F_{TT_3;T'T'_3}(\hat{n})$ are the S^3 sphere harmonic functions.

When a quasiparticle penetrates a HQV loop or pair in the quintet Cooper pairing state, quantum entanglement is generate between them in the final state. We demonstrate this through a concrete example, with the initial state $|i\rangle$ made from a zero charged HQV loop and a quasiparticle with $S_z = \frac{3}{2}$ as

$$|i\rangle = \int_{\hat{n}\in S^3} d\hat{n} \; |\hat{n}\rangle_{vt} \otimes (u \; c^\dagger_{\frac{3}{2}} + v \; c_{-\frac{3}{2}})|\Omega\rangle_{qp}, \tag{39}$$

where $|\Omega\rangle_{qp}$ is the vacuum for Bogoliubov particles. For each phase-sharp state $|\hat{n}\rangle_{vt}$, the particle changes spin according to Eq. 34 in the final state $|f\rangle$. The superposition of non-Abelian phase gives

$$\begin{aligned} |f\rangle &= \int_{\hat{n}\in S^3} d\hat{n} \; \Big\{ u \; (W^\dagger_{11} c^\dagger_{\frac{1}{2}} + W^\dagger_{21} c^\dagger_{-\frac{1}{2}}) + v \; (W^T_{12} c_{\frac{1}{2}} + W^T_{22} c_{-\frac{1}{2}}) \Big\} |\hat{n}\rangle_{vt} \otimes |\Omega\rangle_{qp} \\ &= \int_{\hat{n}\in S^3} d\hat{n} (\hat{n}_3 - i\hat{n}_2) |\hat{n}\rangle_{vt} \otimes (u \; c^\dagger_{\frac{1}{2}} + v \; c_{-\frac{1}{2}})|\Omega\rangle_{qp} \\ &- \int_{\hat{n}\in S^3} d\hat{n} (\hat{n}_1 - i\hat{n}_5) |\hat{n}\rangle_{vt} \otimes (u \; c^\dagger_{-\frac{1}{2}} - v \; c_{\frac{1}{2}})|\Omega\rangle_{qp}. \end{aligned} \tag{40}$$

In terms of the $SO(4)$ quantum numbers, $|i\rangle$ is in a product state as $|00;00\rangle_{vt} \otimes |\frac{1}{2}\frac{1}{2};00\rangle_{qp}$, and $|f\rangle$ is

$$|\frac{1}{2}\frac{1}{2};\frac{1}{2}\frac{-1}{2}\rangle_{vt} \otimes |00;\frac{1}{2}\frac{1}{2}\rangle_{qp} - |\frac{1}{2}\frac{1}{2};\frac{1}{2}\frac{1}{2}\rangle_{vt} \otimes |00;\frac{1}{2}\frac{-1}{2}\rangle_{qp}. \tag{41}$$

In the channel of the (T', T'_3), the final state is exactly an entangled Einstein-Podolsky-Rosen (EPR) pair made up from the HQV loop and the quasi-particle.

5. Quartetting instability in 1D spin-3/2 systems

Quartetting instability is a four-fermion counterpart of the Cooper pairing in spin-3/2 systems, whose order parameter can be written as $O_{qrt}(r) = \psi^\dagger_{\frac{3}{2}}(r)\psi^\dagger_{\frac{1}{2}}(r)\psi^\dagger_{\frac{-1}{2}}(r)\psi^\dagger_{\frac{-3}{2}}(r)$. The quartet is an $SU(4)$ singlet which can be considered as a four-body EPR state. This kind of order is very difficult to analyze in high dimensions because O_{qrt} contains four fermion operators. It lacks of a Bardeen-Cooper-Schrieffer (BCS) type well-controlled mean field theory. Nevertheless, considerable progress has been made in 1D systems. By using Bethe ansatz, Scholttmann [25] showed that the ground state of the $SU(2N)$ model is characterized by the formation of the 2N-particle baryon-like bound state. In contrast, the Cooper pairing can not exist because two particles can not form an $SU(2N)$ singlet.

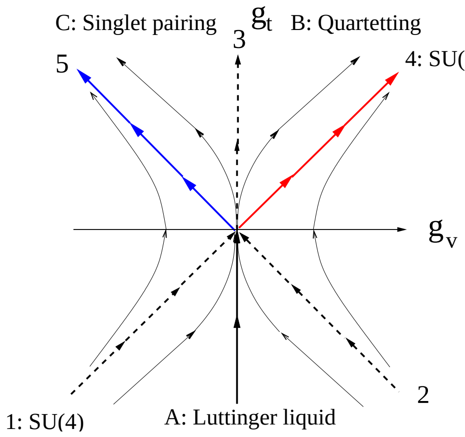

Fig. 6. RG flows in the parameter space (g_v, g_t) in the spin channel. Combined with K_c in the charge channel, they determine various phases as: A) the gapless Luttinger liquid phase, B) quartetting phase with QLRO superfluidity at $K_c > 2$ or $2k_f$ CDW at $K_c < 2$. C) singlet pairing phase with QLRO superfluidity at $K_c < 1/2$ or $4k_f$ CDW at $K_c > 1/2$. They are controlled by the fixed points of $(0, 0)$, $(+\infty, +\infty)$ (line 4), and $(-\infty, +\infty)$ (line 5) respectively. Phase boundaries (line 1, 2, 3) are marked with dashed lines. From Wu Ref. [28].

The strong quantum fluctuations in the spin channel in 1D suppress the Cooper pairing.

In this section we will review the quartetting instability in 1D spin-3/2 systems including the $SU(4)$ symmetric model as a special case [28,36]. We will show that both quartetting and singlet pairing are allowed in different parameter regimes, and study their competitions.

5.1. *Renormalization group and Bosonization analysis*

In 1D systems, we linearize the spectra around the Fermi wavevector k_f, and then decompose the fermion operators into left and right moving parts as $\psi_\alpha = \psi_{R,\alpha} e^{ik_f x} + \psi_{L,\alpha} e^{-ik_f x}$. The right moving currents are also classified into $SO(5)$'s scalar, vector and tensor currents as $J_R(z) = \psi^\dagger_{R,\alpha}(z)\psi_{R,\alpha}(z)$, $J^a_R(z) = \frac{1}{2}\psi^\dagger_{R,\alpha}(z)\Gamma^a_{\alpha\beta}\psi_{R,\beta}(z)$ $(1 \le a \le 5)$, $J^{ab}_R(z) = \frac{1}{2}\psi^\dagger_{R,\alpha}(z)\Gamma^{ab}_{\alpha\beta}\psi_{R,\beta}(z)$ $(1 \le a < b \le 5)$, and the left moving currents can be defined accordingly. The low energy effective Hamiltonian density $\mathcal{H} = \mathcal{H}_0 + \mathcal{H}_{int} + \mathcal{H}'_{int}$ is written as

$$\begin{aligned}
\mathcal{H}_0 &= v_f\Big\{\frac{\pi}{4} J_R J_R + \frac{\pi}{5}(J^a_R J^a_R + J^{ab}_R J^{ab}_R) + (R \to L)\Big\}, \\
\mathcal{H}_{int} &= \frac{g_c}{4} J_R J_L + g_v J^a_R J^a_L + g_t J^{ab}_R J^{ab}_L, \\
\mathcal{H}'_{int} &= \frac{g'_c}{8} J_R J_R + \frac{g'_v}{2} J^a_R J^a_R + \frac{g'_t}{2} J^{ab}_R J^{ab}_R + (R \to L).
\end{aligned} \tag{42}$$

The Umklapp term is absent in this continuum model, whose effects become important in the lattice model at commensurate fillings, and will be discussed in next

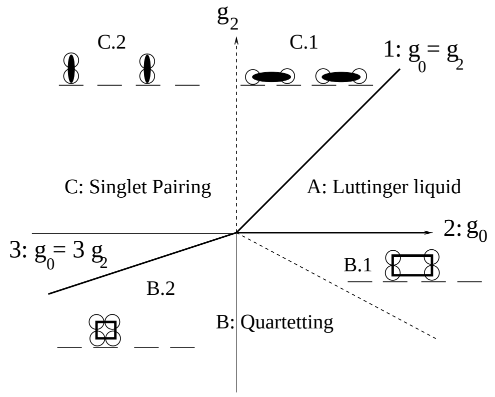

Fig. 7. Phase diagram in terms of the singlet and quintet channel interaction parameters g_0 and g_2. Configurations at quarter filling after the charge gap opens are shown. Phase A is the $SU(4)$ gapless spin liquid. Each of phase B and C splits to two parts. With $g_u \to +\infty$, B.1) quartets with both bond and charge orders, C.1) dimerization of spin Peierls order. With $g_u \to -\infty$, CDW phases of B.2) quartets and C.2) singlet Cooper pairs. Boundaries among phases A, B and C are marked with solid lines, and those between phases B.1 and B.2, and C.1 and C.2 are sketched with dashed lines. From Wu Ref. [28].

section. At the tree level, these dimensionless coupling constants are expressed in terms of g_0, g_2 defined above as

$$g_c = g_c' = \frac{g_0 + 5g_2}{2}, \quad g_v = g_v' = \frac{g_0 - 3g_2}{2}, \quad g_t = g_t' = -\frac{g_0 + g_2}{2}, \tag{43}$$

which are renormalized significantly under the RG process. The chiral terms in H'_{int} only renormalize the Fermi velocities, which can be neglected at the one loop level. At $g_v = g_t$ and $g_v' = g_t'$, or in other words $g_0 = g_2$, the $SU(4)$ symmetry is restored.

The above Hamiltonian Eq. 42 can be bosonized through the identity

$$\psi_{\alpha R,L}(x) = \eta_\alpha / \sqrt{2\pi a} \exp\{\pm i\sqrt{\pi}(\phi_\alpha(x) \pm \theta_\alpha(x))\} \quad (\alpha = \pm\frac{3}{2}, \pm\frac{1}{2}) \tag{44}$$

where the Klein factors η_α are Majorana fermions to ensure the anti-commutation relation among fermions of different species. Boson fields ϕ_α and their dual fields θ_α are conveniently reorganized into ϕ_c (θ_c) in the charge channel, and $\phi_v(\theta_v), \phi_{t1}(\theta_{t1}), \phi_{t2}(\theta_{t2})$ in the spin channels via $\phi_{c,v} = \frac{1}{2}(\phi_{\frac{3}{2}} \pm \phi_{\frac{1}{2}} \pm \phi_{-\frac{1}{2}} + \phi_{-\frac{3}{2}})$, $\phi_{t1,t2} = \frac{1}{2}(\phi_{\frac{3}{2}} \mp \phi_{\frac{1}{2}} \pm \phi_{-\frac{1}{2}} - \phi_{-\frac{3}{2}})$. Similar expressions hold for θ's. In terms of these boson fields, the quadratic part of the Hamiltonian density is standard ($\nu = c, v, t_1, t_2$)

$$\mathcal{H}_0 = \frac{v_\nu}{2} \sum_\nu \Big\{ K_\nu (\partial_x \theta_\nu)^2 + \frac{1}{K_\nu}(\partial_x \phi_\nu)^2 \Big\} \quad \text{with}$$

$$K_\nu = \sqrt{\frac{2\pi v_f + g_\nu' - g_\nu}{2\pi v_f + g_\nu' + g_\nu}}, \quad v_\nu = \sqrt{(v_f + \frac{g_\nu'}{2\pi})^2 - (\frac{g_\nu}{2\pi})^2}, \tag{45}$$

where $g_{t1,t2} = g_t, g'_{t1,t2} = g'_t$. We need to bear in mind that the expression for K_ν, v_ν can not be taken seriously at intermediate and strong couplings where finite but significant renormalizations to K_ν and v_ν take place. The non-quadratic terms are summarized as

$$\begin{aligned}\mathcal{H}_{int} = \frac{-1}{2(\pi a)^2}\Big\{\cos\sqrt{4\pi}\phi_{t1} + \cos\sqrt{4\pi}\phi_{t2}\Big\}\Big\{(g_t + g_v)\cos\sqrt{4\pi}\phi_v \\ + (g_t - g_v)\cos\sqrt{4\pi}\theta_v\Big\} - \frac{g_t}{2(\pi a)^2}\cos\sqrt{4\pi}\phi_{t1}\cos\sqrt{4\pi}\phi_{t2},\end{aligned} \tag{46}$$

with the convention of Klein factors as $\eta_{\frac{3}{2}}\eta_{\frac{1}{2}}\eta_{\frac{-1}{2}}\eta_{\frac{-3}{2}} = 1$. Eq. 46 contains cosine terms of both ϕ_v and its dual field θ_v. Their competition leads to two different spin gap phases with either $\cos\sqrt{4\pi}\phi_v$ or $\cos\sqrt{4\pi}\theta_v$ pinned as shown below. The charge channel c remains quadratic.

The renormalization group (RG) equation of $g_{c,v,c}$ can be calculated from the standard operator product expansion technique [60] as

$$\frac{dg_v}{d\ln(L/a)} = \frac{4}{2\pi}g_v g_t, \quad \frac{dg_t}{d\ln(L/a)} = \frac{1}{2\pi}(3g_t^2 + g_v^2), \quad \frac{dg_c}{d\ln(L/a)} = 0, \tag{47}$$

where L is the length scale and a is the short distance cutoff. Due to the absence of the Umklapp term, the charge part g_c remains unrenormalized at the one-loop level. The $SU(4)$ symmetry is preserved in the RG process along the line $g_v = g_t$. The RG equations can be integrated as $|g_t^2 - g_v^2| = c|g_v|^{3/2}$ (c: constant) with the RG flows as shown in Fig 6. According to the relation Eq. 43, the corresponding boundaries are also shown in Fig. 7.

The phase diagram Fig 6 (Fig. 7) contains three phases at incommensurate fillings. Phase A is the gapless Luttinger liquid phase lying in the repulsive interaction regime with $g_2 < g_0$. All the cosine terms are marginally irrelevant. The leading order divergent susceptibility are the $2k_f$-CDW order $O_{2k_f,cdw} = \psi^\dagger_{R\alpha}\psi_{L\alpha}$, and the $2k_f$-SDW orders in the $SO(5)$ vector channel $N^a = \psi^\dagger_{R\alpha}(\frac{\Gamma^a}{2})_{\alpha\beta}\psi_{L\beta}$, and those in the $SO(5)$ tensor channel $N^{ab} = \psi^\dagger_{R\alpha}(\frac{\Gamma^{ab}}{2})_{\alpha\beta}\psi_{L\beta}$. All of them are with the scaling dimension of $(K_c + 3)/4$.

Phase B is characterized by the formation of quartets. This phase is controlled by the marginally relevant fixed point $g_v = g_s \to +\infty$ (line 4 in Fig. 6), and lies in the regime where attractive interactions dominates (Fig. 7). The spin gap opens with pinned boson fields of ϕ_v, ϕ_{t1} and ϕ_{t2}. The pinned values can be chosen as $\langle\phi_v\rangle = \langle\phi_{t1}\rangle = \langle\phi_{t2}\rangle = 0$ up to a gauge degree of freedom. In phase B, every four fermions first form quartets, then quartets undergo either superfluidity or CDW instabilities. Because the average distance between two nearest quartets is $d = \pi/k_f$, the CDW of quartet is of the $2k_f$-type N. Their order parameters reduce to $O_{2k_f,cdw} \propto e^{i\sqrt{\pi}\phi_c}$ and $O_{qrt} \propto e^{2i\sqrt{\pi}\theta_c}$ respectively. Checking their scaling dimensions $\Delta_N = \frac{1}{4}K_c$ and $\Delta_{qrt} = 1/K_c$, O_{qrt} wins over N at $K_c > 2$. Previous Bethe-ansatz results for the $SU(4)$ case show the quartets formation in Fig. 6 [25]. Here, we extend the quartetting regime to the whole phase B. On the other hand, all the pairing operators $\eta^\dagger$ and $\chi^{a\dagger}$ decay exponentially in phase B.

Phase C is characterized by the formation of the singlet Cooper pairs. The parameter region for this phase is symmetric to phase B in Fig. 6 under the reflection $g_v \to -g_v$. The corresponding fixed point is $-g_v = g_t \to +\infty$. Different from phase B, the dual field θ_v instead of ϕ_v is pinned. Similarly, we can pin the values of bosonic fields $\langle \phi_{t1} \rangle = \langle \phi_{t2} \rangle = \langle \theta_v \rangle = 0$ to minimize the ground state energy. The two leading competing orders in this phase are the singlet pairing $\eta^\dagger$ and the CDW of pairs. This CDW is just the $4k_f$ CDW defined as $O_{4k_f,cdw} = \psi^\dagger_{R\alpha}\psi^\dagger_{R\beta}\psi_{L\beta}\psi_{L\alpha}$. The expressions of these two orders reduce into $\eta^\dagger \propto e^{-i\sqrt{\pi}\theta_c}$, and $O_{4k_f,cdw} \propto e^{\sqrt{4\pi}\phi_c}$. At $K_c > 1/2$, the pairing instability $\eta^\dagger$ wins over the $4k_f$-CDW.

5.2. *Ising transition between quartetting and pairing phases*

Next we study the competition between the quartetting (phase B) and singlet Cooper pairing (phase C), which can be mapped into the phase locking problem of two-component superfluidity [61]. One component is defined as $\Delta^\dagger_1 = \psi^\dagger_{\frac{3}{2}}\psi^\dagger_{\frac{-3}{2}}$, and the other one as $\Delta^\dagger_2 = \psi^\dagger_{\frac{1}{2}}\psi^\dagger_{\frac{-1}{2}}$. Then the singlet pairing operator $\eta^\dagger$ and the quartetting operators are represented as

$$\eta^\dagger = \frac{1}{2}(\Delta^\dagger_1 - \Delta^\dagger_2) \propto e^{i\sqrt{\pi}\theta_c}\cos\sqrt{\pi}\theta_r, \quad O^\dagger_{qrt} = \Delta^\dagger_1\Delta^\dagger_1 = e^{i\sqrt{4\pi}\theta_c}\cos 2\sqrt{\pi}\phi_v, \tag{48}$$

where the charge channel boson field θ_c is the overall phase, and the spin channel boson field θ_v is the relative phase between two components. While $\eta^\dagger$ depends on the relative phase θ_v, $O^\dagger_{qrt}$ depends the dual field ϕ_v.

The overall phase θ_c is always power-law fluctuating in 1D, and does not play a role in the transition. It is the relative phase $\theta_v(\phi_v)$ that controls the transition. The effective Hamiltonian for this transition is a sine-Gordon theory containing cosine terms of both θ_v and ϕ_v as

$$\begin{aligned} H_{res} &= -\frac{1}{2(\pi a)^2}(\lambda_1 \cos\sqrt{4\pi}\phi_v + \lambda_2 \cos\sqrt{4\pi}\theta_v) \quad \text{with} \\ \lambda_{1,2} &= (g_t \pm g_v)(\langle \cos\sqrt{4\pi}\phi_{t1}\rangle + \langle \cos\sqrt{4\pi}\phi_{t2}\rangle). \end{aligned} \tag{49}$$

In phase *C* where $\lambda_1 > \lambda_2$, then the relative phase ϕ_v is locked giving rise to the pairing order. In contrast, in phase *B* where $\lambda_1 < \lambda_2$, the dual field θ_v is locked giving rise to the quartetting order. Along the critical phase boundary line 3 in Fig. 6, $\lambda_1 = \lambda_2$ or ($g_v = 0$), none of θ_v and ϕ_v is pinned. This transition can be mapped into a theory of two Ising fields [62], one of which is at the critical point. Equivalently, it can be regarded as a model with two Majorana fermions, one of which is massless while the other is massive. The Ising order and disorder operators are given by $\cos\sqrt{\pi}\phi_v$ and $\cos\sqrt{\pi}\theta_v$ respectively, both of which have the scaling dimension of $\frac{1}{8}$.

This Ising symmetry breaking effect can also be understood as follows. In addition to the $SO(5)$ symmetry, spin-3/2 systems have another Z_2 symmetry in the spin channel $U_n = e^{in_4\pi}$ under which ψ_α, $\eta^\dagger$, and O_{qrt} transform as

$$\begin{aligned} U_n \psi_{\pm\frac{3}{2}} U_n^{-1} &= i\psi_{\pm\frac{3}{2}}, \quad U_n \psi_{\pm\frac{1}{2}} U_n^{-1} = -i\psi_{\pm\frac{1}{2}}, \\ U_n \eta^\dagger U_n^{-1} &= -\eta, \qquad U_n O_{qrt} U_n^{-1} = O_{qrt}. \end{aligned} \tag{50}$$

This Z_2 transformation shifts the relative phase θ_v as $\sqrt{\pi}\theta_v \to \sqrt{\pi}\theta_v \pm \pi$ but leaves $\sqrt{\pi}\phi_v$ unchanged. Thus this Z_2 symmetry is broken in the singlet pairing phase B, but is kept in the quartetting phase C.

5.3. *Discussion of quartetting in high dimensions*

The study of quartetting phase, or the more general multi-particle clustering instabilities in high dimensions is a challenging problem. Ropke *et al.* [63] compared the instabilities of deuteron (pairing) and α-particle (quartetting) channel in nuclear physics using diagrammatic method. They found that at low density or strong interaction strength, the α-particle instability wins over the deuteron instability. Stepnaneko *et al.* [26] constructed a trial wavefunction in 3D to describe the quartetting order. Lee [29] studied the 2D ground state binding energy of the N-particle cluster in the $SU(N)$ case.

In high dimensions, the competition between quartetting and pairing superfluidities is more complicated than that in 1D. First, the pairing superfluidity breaking spin rotational symmetry can not be stabilized at 1D, but can exist at $D \geq 2$. Second, phase transitions from weak to strong coupling regimes can take place at $D \geq 2$ unlike in 1D interactions always renormalize into strong coupling regime. Taking into account these facts, we discuss the symmetry class of these competitions. We begin with the $SU(4)$ line with $g_0 = g_2 = g < 0$. At weak coupling, the sextet pairing state ($\eta^\dagger$ and $\chi^\dagger$ are degenerate) is stabilized breaking the $U(1)$ charge symmetry and also the $SU(4)$, or isomorphically $SO(6)$ symmetry in the spin channel. The residue symmetry is $[SO(5) \ltimes Z_2] \otimes Z_2$. The first Z_2 is a combined spin-phase operation which flips the direction of the pairing operator in the spin channel and simultaneously shift the phase by π, which is of the same nature responsible for the HQV in the quintet superfluid in Sect. 4. The second Z_2 is purely the phase operation $\psi_\alpha \to -\psi_\alpha$ which leave pairing operators unchanged. On the other hand, the quartetting state in the strong coupling limit is $SU(4)$ invariant, and also breaks the $U(1)$ symmetry. Its residue symmetry is $SO(6) \otimes Z_4$ where Z_4 operation means $\psi_\alpha \to e^{im\pi/2}\psi_\alpha (m = 1 \sim 4)$. Thus this phase transition is describe by the coset $SO(6) \otimes Z_4/[SO(5) \ltimes Z_2 \otimes Z_2] = S^5$. In other words, the pairing to quartetting transition can be viewed as an order to disorder transition of pairing operators for their spin configuration on the S^5 sphere. If the spin configuration becomes disordered, due to the combined spin-phase Z_2 structure, the phase of the pair operators is only well defined modulo of π, thus it means the quartetting order appears. If $g_2 < g_0 < 0$ or $g_0 < g_2 < 0$, then in the weak coupling limit, the quintet pairing state $\chi^\dagger$, or the singlet pairing $\eta^\dagger$ dominates. A similar reasoning shows that the coset for the transition from the quartetting state to the quintet or singlet Cooper pairing states is S^4 or Z_2, respectively.

6. Magnetic properties in spin-3/2 systems

In the strong repulsive interaction regime $U_0,\ U_2 \gg t$ and at commensurate fillings, the low energy physics of spin-3/2 systems are described by the magnetic exchange models. In this section, we review the magnetic properties in such systems[28,37], and also present new results in Sect. 6.3 and 6.4.

6.1. *Magnetic exchange at quarter-filling*

We first construct the exchange Hamiltonian at quarter-filling i.e., one particle per site. The total spin of two sites in a bond can be $S_{tot} = 0, 1, 2, 3$. Using the projection perturbation theory, we find the exchange exchange energy in each channel as

$$J_0 = \frac{4t^2}{U_0}, \quad J_2 = \frac{4t^2}{U_2}, \quad J_1 = J_3 = 0, \tag{51}$$

where the degeneracy of $J_{1,3}$ is a consequence of the $SO(5)$ symmetry. This model can be represented in the standard Heisenberg type by using bi-linear, bi-quadratic, and bi-cubic terms as $H_{ex} = \sum_{ij} a\ (\vec{S}_i \cdot \vec{S}_j) + b\ (\vec{S}_i \cdot \vec{S}_j)^2 + c\ (\vec{S}_i \cdot \vec{S}_j)^3$, with $a = -\frac{1}{96}(31J_0 + 23J_2)$, $b = \frac{1}{72}(5J_0 + 17J_2)$ and $c = \frac{1}{18}(J_0 + J_2)$. More elegantly, it can be represented in the explicit $Sp(4)$ symmetric form as

$$H_{ex} = \sum_{ij} \Big\{ \frac{J_0 + J_2}{4} L_{ab}(i)L_{ab}(j) + \frac{3J_2 - J_0}{4} n_a(i)n_a(j) \Big\}. \tag{52}$$

Eq. 52 satisfies two different $SU(4)$ symmetries at $J_0 = J_2$ and $J_2 = 0$, respectively. The first one denoted as $SU(4)_A$ below is obvious at $J_0 = J_2$ where Eq. 52 reduces into the $SU(4)$ Heisenberg model of $H_{SU(4),A} = \sum_{ij} \frac{J}{2} \Big\{ L_{ab}(i)L_{ab}(j) + n_a(i)n_a(j) \Big\}$. Each site is in the fundamental representation. The second $SU(4)$ symmetry exists in the bipartite lattice at $J_2 = 0$ denoted as $SU(4)_B$ below. We perform a particle-hole transformation in the odd sublattice $L'_{ab} = L_{ab},\ n'_a = -n_a$, i.e., the odd sites are transformed into the anti-fundamental representation. Eq. 52 is again $SU(4)$ invariant as

$$H_{SU(4),B} = \sum_{ij} \frac{J_0}{4} \Big\{ L'_{ab}(i)L_{ab}(j) + n'_a(i)n_a(j) \Big\}, \tag{53}$$

but with fundamental and anti-fundamental representations alternatively in even and odd sites. This $SU(4)_B$ model and the more generally staggered $SU(N)$ Heisenberg model were investigated extensively by using the large N method [64,65]. These two $SU(4)$ symmetries have dramatically different physical properties. At least four sites are needed to form an $SU(4)$ singlet for the $SU(4)_A$, while for $SU(4)_B$, two sites are enough to form a bond singlet.

6.2. *1D phases at quarter-filling*

The phase diagram of Eq. 52 at 1D can be obtained by using the bosonization method to the Hubbard model. At quarter-filling, the $8k_f$ term Umklapp term is important and only involves the charge sector. It can be bosonized as

$$\mathcal{H}_{um,8k_f} = \frac{g_u}{2(\pi a)^2} \cos(\sqrt{16\pi}\phi_c - 8k_f x), \tag{54}$$

where g_u is at the order of $O(g_0^3, g_2^3)$ at the bare level. At quarter-filling, the spin channels behave the same as in the incommensurate case discussed in Sect. 5.1. The charge channel opens up the gap at $K_c < 1/2$ where g_u is renormalized to infinity. As a result, the degeneracy between the real and imaginary parts of the $O_{2k_f,cdw}$ and $O_{4k_f,cdw}$, are lifted. Their real parts describe the usual CDW orders, while their imaginary parts mean the bond orders, i.e., the $2k_f$ and $4k_f$ spin Peierls orders.

With the opening of charge gap at quarter-filling, various insulating phases appear as given in Fig. 7. Phase A and C1 corresponds to the regime described by the exchange model Eq. 52 with $J_2 \geq J_0$ and $J_2 < J_0$, respectively. Phase A ($J_2 \geq J_0 > 0$), including the $SU(4)_A$ line, is a gapless spin liquid phase. The $SU(4)_A$ line was solved by Sutherland [66]. In phase C.1 ($J_2 \leq J_0$), the spin gap opens with the developing of the $4k_f$ spin-Peierls order, i. e., the dimer order. The transition between these two phases is Kosterlitz-Thouless like. Insulating phases involving CDW order also exist in phases B.1, B.2 and C.2. The quartetting phase B splits into two parts B.1 and B.2. In phase B.1, the $SU(4)$ singlet quartets exhibit both the charge and spin Peierls orders. In phase B.2, the $2k_f$ CDW of quartets becomes long range ordered. Similarly, the CDW of singlet pairs becomes long range ordered in phase C.2. The boundaries between phase B.1 and B.2, phase C.1 and C.2 are determined by the bare value of $g_{u0} = 0$ as sketched in Fig. 7. However, due to the non-universal relations between g_{u0} and $g_{0,2}$, the exact boundaries are hard to determine.

6.3. *Discussion of the 2D phase diagram at quarter-filling*

The 2D physics of Eq. 52 is a challenging problem. Nevertheless, good understanding has been achieved for the $SU(4)_B$ line ($J_2 = 0$) in the square lattice where both quantum Monte-Carlo simulations [67] and the large-N analysis show that the ground state [65,68] is long range Neel ordered. As a result of strong quantum fluctuations, the Neel moments are $(-)^i n_4 = (-)^i L_{15} = (-)^i L_{34} \approx 0.05$, which is really tiny compared to the $SU(2)$ case. The Goldstone manifold is $CP(3) = U(4)/[U(1) \otimes U(3)]$ with 6 branches of spin-waves.

However, the physics is less clear away from the $SU(4)_B$ line. The $SU(4)_A$ line of $J_0 = J_2$ is of particular interest. In order to form a singlet for $SU(4)_A$, we need four sites around a plaquette with the wavefunction of $\frac{1}{4!}\epsilon_{\alpha\beta\gamma\delta}\psi^\dagger_\alpha(1)\psi^\dagger_\beta(2)\psi^\dagger_\gamma(3)\psi^\dagger_\delta(4)|\Omega\rangle$ where $|\Omega\rangle$ is the vacuum. Indeed, an exact diagonalization by Bossche *et al.* in a 4×4

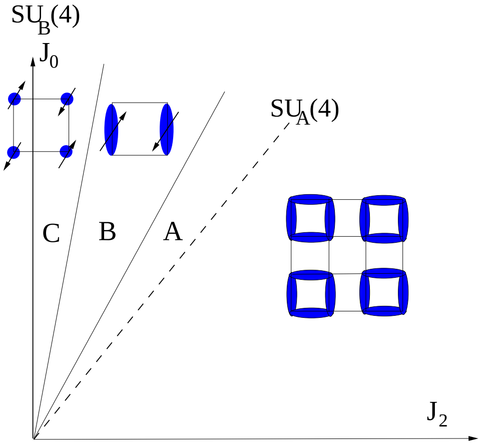

Fig. 8. Speculated phase diagram at quarter-filling in a 2D square lattice. Phase A is the plaquette ordered phase which is suggested along the $SU(4)_A$ line in an exact diagonalization work by Bossche et al. [67] Phase C is the Neel ordered phase which is confirmed along the $SU(4)_B$ line in QMC simulations by Harada et al. [65] We speculate a dimerized phase B lying between phase A and C. Dimers in phase B carry antiferromagnetic spin-nematic order.

sites lattice [69] suggests that the ground state along the $SU(4)_A$ line exhibits such plaquette order as depicted in Fig. 8. This plaquette order was also found in a large-N mean field theory by Mishra *et al* [70]. However, due to the sign problem in QMC, a large size simulation is difficult to confirm this result. Recently, Chen *et al* [37] constructed an $SU(4)$ Majumdar-Ghosh model in a two-leg spin-3/2 ladder whose ground state is solvable exhibiting this plaquette state. Similarly to the quartetting order in the superfluid state, this plaquette order is of four sites without any site and bond spin orders. Upon doping, we suggest that a quartetting superfluid appears.

Now let us speculate the phase diagram in the entire parameter regime as depicted in Fig. 8. We expect that the long range Neel order can survive with a finite value of J_2 as marked as phase C in Fig. 8. The plaquette ordered phase is gapped, thus it should be stabilized in an entire phase as marked phase C. It extends into a finite regime with $J_2 < J_0$, and we also speculate that it survives in the entire region of $J_0 < J_2$. Furthermore, between phase C with the site spin order and phase A with the plaquette spin order, we suggest the existence of the magnetically ordered dimer phase B. The dimer made of two spin-3/2 particles possesses the internal spin structures. In phase B where $J_2 < J_0$, the energy of the dimer singlet state is lower than the energy of the dimer quintet. Their superposition might give rise to an antiferromagnetically ordered spin-nematic dimer state. More analytic and numeric works are desired to confirm these speculations.

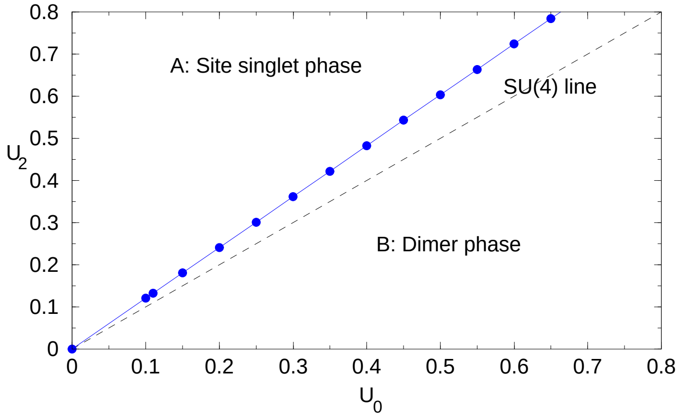

Fig. 9. 1D phase diagram at half-filling (two particles per site) with $U_{0,2} > 0$ (t is rescaled to 1). The phase boundary is marked with the solid line, and the $SU(4)$ line ($U_0 = U_2$) is marked with the dashed line. A) The site singlet phase; B) The spin-Peierls (dimer) phase.

6.4. *spin-3/2 magnetism at half-filling*

At half-filling with $U_0, U_2 \gg t$, the exchange model has been derived as Eq. 19. In 1D, the phase diagram of Eq. 19 can be obtained by applying the bosonization method directly to the Hubbard model after taking into account the $4k_f$-Umklapp terms as

$$\mathcal{H}_{um,4k_f} = \frac{\lambda_s}{2}\eta_R^\dagger \eta_L + \frac{\lambda_v}{2}\chi_R^a \chi_L^a + h.c., \tag{55}$$

where $\eta_R = \psi^\dagger_{R\alpha} R_{\alpha\beta} \psi^\dagger_{R\beta}$, $\chi_R = \psi^\dagger_{R\alpha}(R\Gamma^a)_{\alpha\beta}\psi^\dagger_{R\beta}$, and η_L, χ_L are defined correspondingly. The bare values for $\lambda_{s,v}$ are $\lambda_s = U_0 a_0, \lambda_v = U_2 a_0$ where a_0 is the lattice constant. This term can be bosonized as

$$\begin{aligned}\mathcal{H}_{um,4k_f} = &-\frac{1}{2(\pi a)^2}\cos(\sqrt{4\pi}\phi_c)\Big\{(\lambda_v + \lambda_s)\cos\sqrt{4\pi}\phi_v + (\lambda_v - \lambda_s)\cos\sqrt{4\pi}\theta_v \\ &+ 2\lambda_v(\cos\sqrt{4\pi}\phi_{t1} + \cos\sqrt{4\pi}\phi_{t2})\Big\},\end{aligned} \tag{56}$$

Together with Eq. 42, the RG equations at the half-filling can be calculated as

$$\begin{aligned}\frac{dg_c}{d\ln t} &= \frac{1}{2\pi}(\lambda_s^2 + 5\lambda_v^2), & \frac{dg_v}{d\ln t} &= \frac{1}{2\pi}(4g_v g_t + 2\lambda_s\lambda_v), \\ \frac{dg_t}{d\ln t} &= \frac{1}{2\pi}(3g_t^2 + g_v^2 + 2\lambda_v^2), & \frac{d\lambda_s}{d\ln t} &= \frac{1}{2\pi}(g_c\lambda_s + 5g_v\lambda_v), \\ \frac{d\lambda_v}{d\ln t} &= \frac{1}{2\pi}(g_c\lambda_v + g_v\lambda_s + 4g_t\lambda_v). \end{aligned} \tag{57}$$

Eq. 57 are solved numerically in the region $U_0 > 0, U_2 > 0$. Two stable fixed points are found as

$$\mathrm{A}: g_c = -g_v = g_t = -\lambda_s = \lambda_v \to +\infty, \quad \mathrm{B}: g_c = g_v = g_t = \lambda_s = \lambda_v \to +\infty. \tag{58}$$

with the corresponding phase diagram shown in Fig. 9. Phase A is the site singlet phase with the pinned values of the boson fields as $\langle\phi_c\rangle = \langle\theta_v\rangle = \langle\phi_{t1}\rangle = \langle\phi_{t2}\rangle = 0$. All the charge orders and spin-Peierls orders vanish in this phase. Phase B is the dimerized phase with pinned boson fields as $\langle\phi_c\rangle = \langle\phi_v\rangle = \langle\phi_{t1}\rangle = \langle\phi_{t2}\rangle = 0$. As a result, the $2k_f$ spin-Peierls (dimer) order is long range ordered. We notice that the $SU(4)$ line of $U_0 = U_2$ is already inside the dimer phase, thus is not critical. This agrees with the previous RG result in Ref. [71]. The phase boundary is determined by numerically solving the above RG equations, which extends to the region with $U_0 < U_2$. The transition between phase A and B is Ising-like, which is driven by the competitions between ϕ_v and θ_v.

The two dimension phase diagram of Eq. 19 is also challenging. As discussed in Sect. 3.3, at $U_0 < U_2$ Eq. 19 reduces to the $SO(5)$ rotor model. When the difference between U_2 and U_0 is small, or large compared to the inter-site exchange, the system is in the antiferromagnetic spin-nematic phase, or in the site singlet phase. In the regime of $U_2 \leq U_0$, it is not clear whether the ground state still possesses magnetic long range order. An interesting numeric QMC result [72] showed that along the $SU(4)$ line, Eq. 19 is in the gapless spin liquid phase, but more numeric work is desirable to confirm it.

7. Summary

In summary, we have reviewed the hidden $SO(5)$ symmetry in spin-3/2 cold atomic systems. This symmetry is proved to be exact in the continuum model with *s*-wave interactions, and in the lattice Hubbard model in the optical lattices. This high symmetry provides a framework to understand various properties in spin-3/2 systems, including the Fermi liquid theory, mean field phase diagram, and the sign problem in QMC simulations. spin-3/2 systems support novel superfluid states including the quintet Cooper pairing state and the quartetting state. The topological defect of half-quantum vortex and the $SO(4)$ Cheshire charge effect were discussed in the quintet superfluid. The existence of the quartetting state in 1D systems and its competition with the Cooper pairing state were investigated. At last, we reviewed the magnetism in spin-3/2 systems showing many different features from the spin-$\frac{1}{2}$ systems.

Taking into account the rapid progress in the cold atomic physics, we are optimistic that the spin-3/2 high spin cold atomic systems can be realized in experiment in the near future. We hope that the research on the hidden symmetry aspect can stimulate general interest in various properties in such systems.

Acknowledgments

I thank my Ph. D advisor S. C. Zhang for his guidance on the research in spin-3/2 cold atoms, and L. Balents, C. Capponi, S. Chen, J. P. Hu, O. Motrunich, Y. P. Wang for collaborations on this topic. I also thank H. D. Chen, E. Demler, L. M. Duan, E. Fradkin, M. P. A. Fisher, T. L. Ho, A. J. Leggett, M. Ma, D. Scalapino,

M. Troyer, J. Zaanen, and F. Zhou for helpful discussions. This work is supported by the NSF Grant No. Phy99-07949.

References

1. M. H. Anderson *et al.*, Science **269**, 198 (1995).
2. K. B. Davis *et al.*, Phy. Rev. Lett. **74**, 5202 (1995).
3. C. J. Myatt *et al.*, Phys. Rev. Lett. **78**, 586 (1997).
4. D. M. Stamper-Kurn *et al.*, Phys. Rev. Lett. **80**, 2027 (1998).
5. J. Stenger *et al.*, Nature **396**, 345 (1998).
6. M. Greiner *et al.*, Nature **415**, 39 (2002).
7. T. L. Ho, Phys. Rev. Lett. **81**, 742 (1998).
8. T. Ohmi and K. Machida, J. Phys. Soc. Jpn. **67**, 1822 (1998).
9. F. Zhou, Phys. Rev. Lett. **87**, 80401 (2001).
10. F. Zhou, Int.Jour.Mod.Phys.B17 **17**, 2643 (2003).
11. E. Demler and F. Zhou, Phys. Rev. Lett. **88**, 163001 (2002).
12. F. Zhou and M. Snoek, Annals of Physics **308**, 692 (2003).
13. A. Imambekov, M. Lukin, and E. Demler, Phys. Rev. A **68**, 63602 (2003).
14. A. Widera *et al.*, cond-mat/0604038, unpublished.
15. F. Zhou and G. W. Semenoff, cond-mat/0607463, unpublished.
16. A. Griesmaier *et al.*, Phys. Rev. Lett. **94**, 160401 (2005).
17. J. Stuhler *et al.*, Phys. Rev. Lett. **95**, 150406 (2005).
18. R. B. Diener and T. L. Ho, Phys. Rev. Lett. **96**, 190405 (2006).
19. L. Santos and T. Pfau, cond-mat/0510634, unpublished.
20. S. K. Yip and T. L. Ho, Phys. Rev. A **59**, 4653 (1999).
21. C. Wu, J. P. Hu, and S. C. Zhang, Phys. Rev. Lett. **91**, 186402 (2003).
22. S. C. Zhang, Science **275**, 1089 (1997).
23. C. Wu and S. C. Zhang, Phys. Rev. B **71**, 155115 (2005).
24. C. Wu, J. P. Hu, and S. C. Zhang, cond-mat/0512602, unpublished.
25. P. Schlottmann, Journal of Physics-Condensed Matter **6**, 1359 (1994).
26. A. S. Stepanenko and J. M. F. Gunn, cond-mat/9901317, unpublished.
27. H. Kamei and K. Miyake, J. Phys. Soc. Jpn. **74**, 1911 (2005).
28. C. Wu, Phys. Rev. Lett. **95**, 155115 (2005).
29. D. Lee, Phys. Rev. A **73**, 63204 (2006).
30. A. Rapp, G. Zarand, C. Honerkamp, and W. Hofstetter, cond-mat/0607138, unpublished.
31. C. Honerkamp and W. Hofstetter, Phys. Rev. Lett. **92**, 170403 (2004).
32. C. A. Regal, M. Greiner, and D. S. Jin, Phys. Rev. Lett. **92**, 40403 (2004).
33. M. W. Zwierlein *et al.*, Phys. Rev. Lett. **92**, 120403 (2004).
34. J. Kinast *et al.*, Phys. Rev. Lett. **92**, 150402 (2003).
35. M. Bartenstein *et al.*, Phys. Rev. Lett. **92**, 203201 (2004).
36. P. Lecheminant, E. Boulat, and P. Azaria, Phys. Rev. Lett. **95**, 240402 (2005).
37. S. Chen, C. Wu, Y. P. Wang, and S. C. Zhang, Phys. Rev. B **72**, 214428 (2005).
38. M. Machholm, P. S. Julienne, and K. A. Suominen, Phys. Rev. A **64**, 33405 (2001).
39. R. Maruyama, Bull. Am. Phys. Soc. **48**, 27 (2003).
40. Y. Takasu *et al.*, Phys. Rev Lett **90**, 23003 (1975).
41. Y. Takasu *et al.*, Phys. Rev Lett **91**, 40404 (2003).
42. L. W. He *et al.*, Phys. Rev. Lett. **67**, 2131 (1991).
43. K. Hattori, J. Phys. Soc. Jpn. **74**, 3135 (2005).
44. D. Controzzi and A. M. Tsvelik, Phys. Rev. Lett. **96**, 97205 (2006).

45. T. L. Ho and S. Yip, Phys. Rev. Lett. **82**, 247 (1999).
46. S. Murakami, N. Nagaosa, and S. C. Zhang, Phys. Rev. B **69**, 235206 (2004).
47. C. N. Yang and S. C. Zhang, Mod. Phys. Lett. **4**, 769 (1990).
48. H. H. Lin, L. Balents, and M. P. A. Fisher, Phys. Rev. B **58**, 1794 (1998).
49. R. Konik and A. W. W. Ludwig, Phys. Rev. B **64**, 155112 (2001).
50. R. Blankenbecler, D. J. Scalapino, and R. L. Sugar, Phys. Rev. D **24**, 2278 (1981).
51. S. Capponi, C. Wu, and S. C. Zhang, Phys. Rev. Lett. **70**, 220505(R) (2004).
52. S. E. Koonin, D. J. Dean, and K. Langanke, Phys. Rep. **278**, 1 (1997).
53. S. Hands *et al.*, Eur. Phys. J. C **17**, 285 (2000).
54. I. J. R. Aitchison, Phys. Rev. B **51**, 6531 (1995).
55. M. Stone, Int. Jour. Mod. Phys. B **9**, 1359 (1995).
56. A. J. Leggett, Reviews of Modern Physics **47**, 331 (1975).
57. A. S. Schwarz, Nucl. Phys. B **208**, 141 (1982).
58. M. Bucher, K. M. Lee, and J. Preskill, Nucl. Phys. B **386**, 27 (1999).
59. P. McGraw, Phys. Rev. D **50**, 952 (1994).
60. D. Senechal, cond-mat/9908262.
61. A. J. Leggett, Prog. Theo. Phys. **36**, 901 (1966).
62. H. J. Schulz, Phys. Rev. B **53**, R2959 (1996).
63. G. Ropke, A. Schnell, P. Schuck, and P. Nozieres, Phys. Rev. Lett. **80**, 3177 (1998).
64. D. P. Arovas and A. Auerbach, Phys. Rev. B **38**, 316 (1988).
65. N. Read and S. Sachdev, Phys. Rev. B **42**, 4568 (1990).
66. B. Sutherland, Phys. Rev. B **12**, 3795 (1975).
67. K. Harada, N. Kawashima, and M. Troyer, Phys. Rev. Lett. **90**, 117203 (2003).
68. G. M. Zhang and S. Q. Shen, Phys. Rev. Lett. **87**, 157201 (2001).
69. M. V. D. Bossche, F. C. Zhang, and F. Mila, Eur. Phys. J. B **17**, 367 (2000).
70. A. Mishra, M. Ma, and F. C. Zhang, Phys. Rev. B **65**, 214411 (2002).
71. R. Assaraf *et al.*, Phys. Rev. Lett. **93**, 016407 (2004).
72. F. F. Assaad, Phys. Rev. B **71**, 75103 (2005).